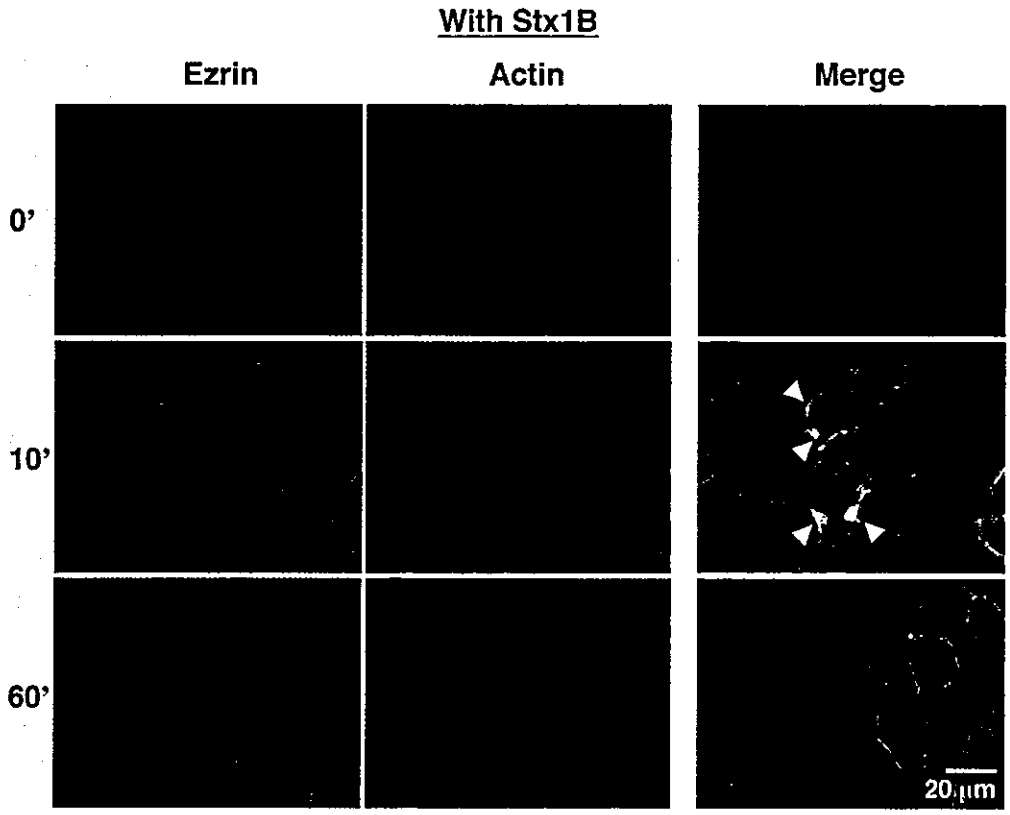

Fig. 2. Effect of Stx1-B subunit on the distribution of ezrin and actin in ACHN cells. ACHN cells treated with the Stx1-B subunit as described in Fig. 1 were double-stained with Alexa-488-labeled anti-ezrin mAb (left panels, green) and TRITC-phalloidin (center panels, red) and visualized using confocal microscopy. The right panels represent the superposition of the green and red images, with DAPI counter staining (blue). The arrowheads indicate the areas of ezrin and actin colocalization (yellow). Results are representative of five independent experiments.

was concentrated in the margin of the cells, as revealed by the brush-like meshwork (Fig. 2, top panels). However, Stx1-B treatment induced a transient enhancement in the concentration of ezrin just beneath the plasma membrane (Fig. 2). Occasionally, the protein clustering peaked at 10 minutes after Stx1-B stimulation (Fig. 2). In parallel, the cortical actin filaments were temporarily polymerized and appeared as thick bundles at the margin of the cells (Fig. 2). The colocalization of both proteins peaked at 10 minutes after Stx1-B stimulation (Fig. 2, yellow area, indicated by arrowhead).

As ERM proteins are thought to play a central role in the organization of cortical actin-based cytoskeletons through the cross-linking of actin filaments and integral membrane, such as CD44 (Tsukita et al., 1994; Tsukita and Yonemura, 1999), we next examined the changes in the distribution of CD44 induced by Stx1-B treatment. As with ezrin, Stx1-B treatment temporarily enhanced the concentration of CD44 in the cell membrane of ACHN cells (Fig. 3). Dual staining with CD44 and F-actin revealed a significant colocalization of both proteins that peaked at 10 minutes after Stx1-B stimulation (Fig. 3, yellow area, indicated by arrowhead).

Paxillin and FAK have been shown to be important for the focal adhesion of cells and growth factor-induced morphological changes (Burridge et al., 1992; Leventhal et al., 1997). Therefore, we examined the effect of Stx1-B stimulation on the distribution of FAK and paxilin. As shown in Fig. 4, most of the FAK and paxillin proteins were independently disseminated throughout the cytoplasm, while small portions of both proteins were colocalized and concentrated within a distinct radial streak at the edges of the cell lamella (yellow area). Upon the addition of Stx1-B, however, the colocalization of FAK and paxillin was temporally enhanced, peaking at 10 minutes after stimulation (Fig. 4, arrowhead).

We further examined the effect of Stx1-B stimulation on other cytoskeletal proteins. The distributions of vimentin and cytokeratin were similar, appearing as a diffuse localization with radial meshwork in the cytoplasm of resting ACHN cells (Fig. 5). Upon Stx1-B stimulation, however, both proteins were temporary concentrated within a paranuclear lesion, peaking at 30 minutes after stimulation in a synchronous manner (Fig. 5, arrowhead).

When the distribution of tubulins was examined using fluorescence immunohistochemistry, a fine mesh work of α-tubulin was seen within the cytoplasm of ACHN cells (Fig. 6). Upon Stx1-B stimulation, the α-tubulin filaments became significantly polymerized, appearing as a thickening of the bundles throughtout the entire cytoplasm and peaking at 10 minutes after stimulation (Fig. 6). Conversely, γ-tubulin was found in cytoplasmic complexes identified as fine spots and specifically concentrated at microtubule-organizing centers (Moritz and Agard, 2001) (Fig. 6). Although the distribution of γ-tubulin did not change significantly after Stx1-B stimulation, a slight enhancement at the microtubule-organizing centers was observed (Fig. 6, arrowhead).

All above observations on Stx1-B-induced cytoskeletal remodeling are entirely based on imaging studies. Therefore, we next examined F-actin formation after Stx1-B stimulation by biochemical means. For this purpose, cell lysate prepared by using actin stabilization buffer was centrifuged and F-actin fraction was separated from soluble G-actin fraction as the pellet. As shown in Fig. 7A, quantification by densitometry of

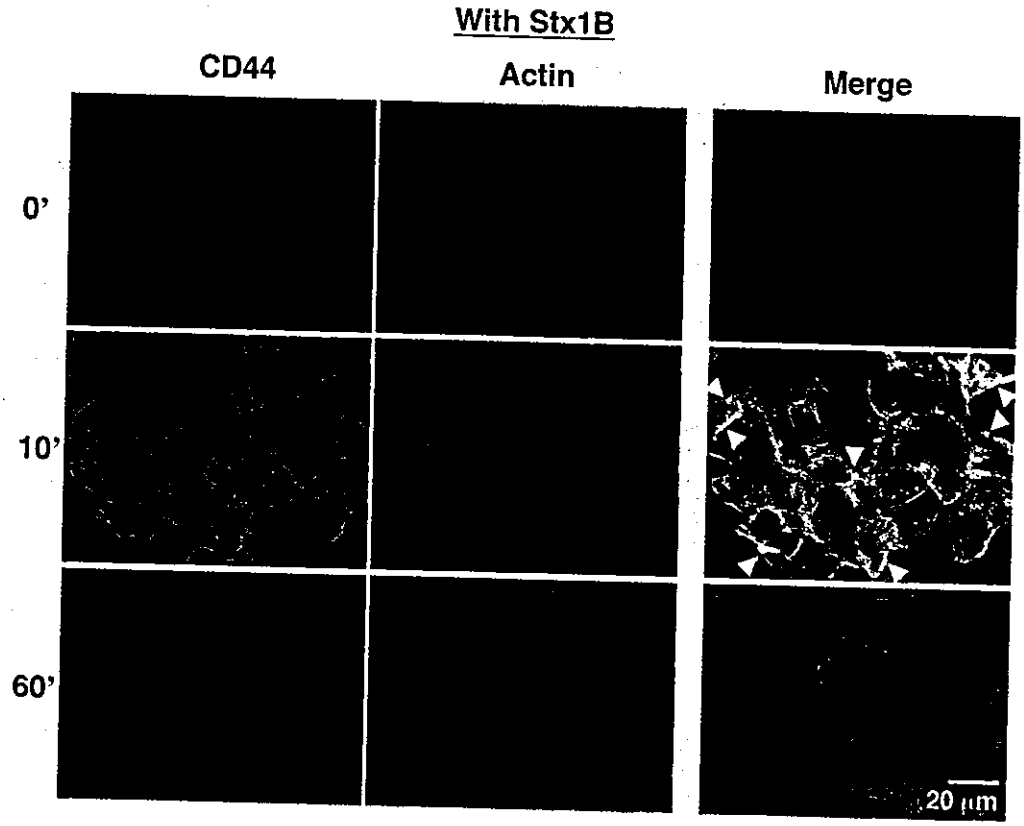

3. Effect of Stx1-B subunit on
istribution of CD44 and actin
HN cells. ACHN cells were
ined as described in Fig. 2
; Alexa-488-labeled anti-
4 mAb (left panels, green)
RITC-phalloidin (center
s, red). The arrowheads
ate the areas of CD44 and
colocalization (yellow).
lts are representative of three
endent experiments.

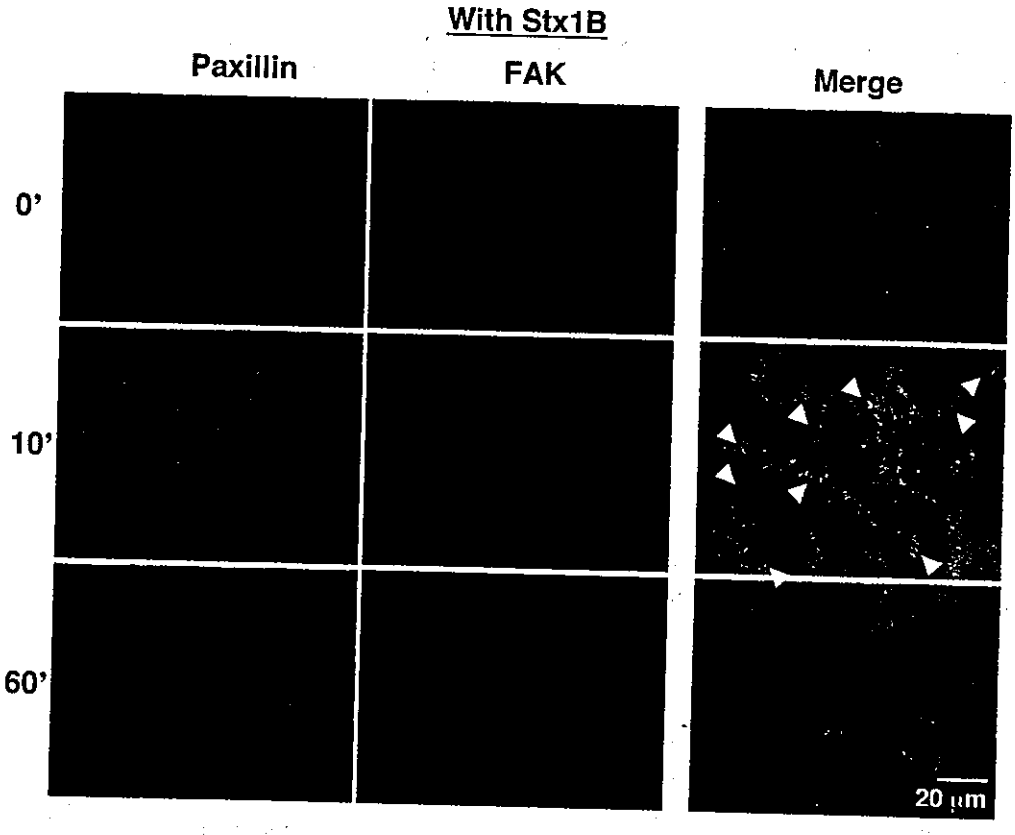

Effect of Stx1-B subunit on
tribution of paxillin and
ı ACHN cells. ACHN cells
xamined as described in
ısing Alexa-488-labeled
xillin mAb (left panels,
and Alexa-546-labeled
.K Ab (center panels, red).
owheads indicate the areas
llin and FAK colocalization
). Results are
ntative of three
ident experiments.

oblots revealed a transient increase in the amount of F-
action, which peaked at 10 to 30 minutes after Stx1-B
tion. These data coincide with those observed by confocal microscopy experiments using fluorescently labeled phalloidin as a probe for F-actin (Figs 2, 3). We also examined tubulin polymerization similarly. As shown in Fig. 7B, Stx1-

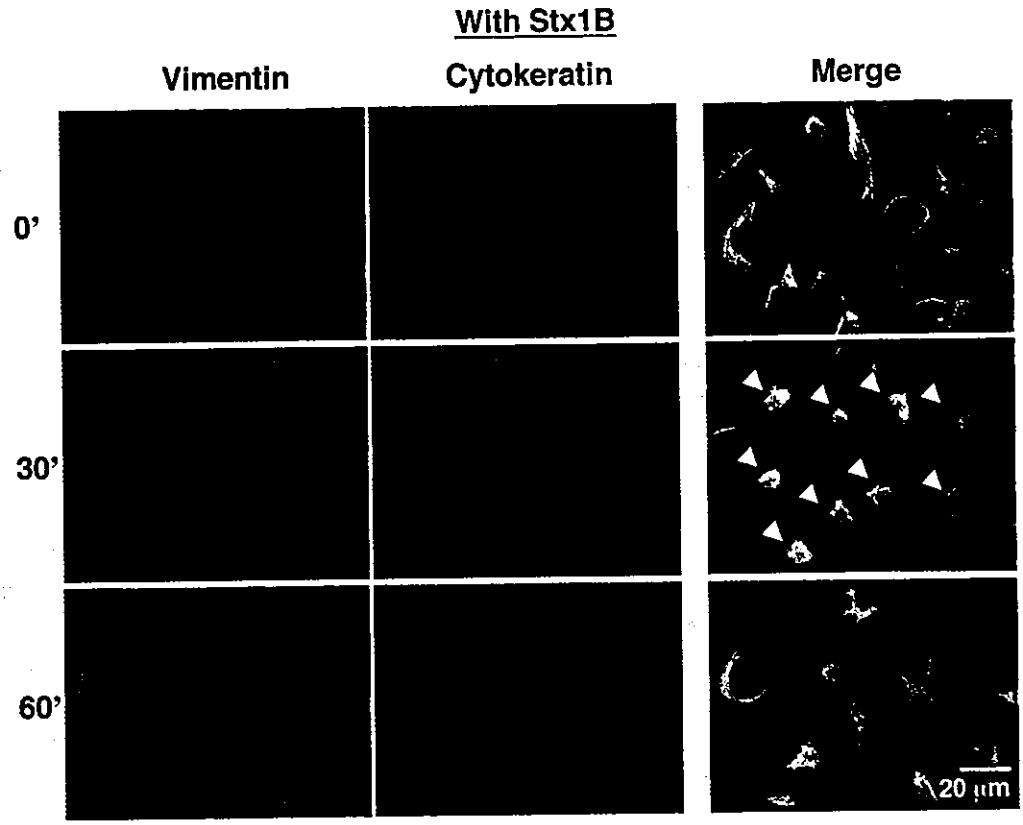

Fig. 5. Effect of Stx1-B subunit on the distribution of vimentin and cytokeratin in ACHN cells. ACHN cells were examined as described in Fig. 2 using Alexa-488-labeled anti-vimentin mAb (left panels, green) and Alexa-546-labeled anti-cytokeratin mAb (center panels, red). The arrowheads indicate the perinuclear clustering of vimentin. Results are representative of three independent experiments.

B-induced transient tubulin polymerization was also confirmed by quantitative analysis.

Stx1-B induces transient phosphorylation of ezrin

The phosphorylation of cytoskeletal proteins plays a key role in cytoskeletal remodeling (Tsukita and Yonemura, 1999). Thus, we attempted to examine whether the phosphorylation state of the cytoskeletal proteins changes. When the total cell lysates prepared from Stx1-B-treated ACHN cells were examined using immunoblotting with Abs that specifically recognize Src family PTKs only when activated by phosphorylation at the C-terminal tyrosine residue, the intensification of three major bands was seen after Stx1-B treatment (Fig. 8A). Based on the molecular weights, the largest band was thought to represent the activated form of Yes, which was previously reported to appear during the course of Stx1-B-mediated activation in ACHN cells (Katagiri et al., 1999; Katagiri et al., 2001). The other smaller bands were thought to represent the activation of other Src family PTK(s) by Stx1-B stimulation. In parallel with the activation of Src family PTKs, the Stx1-B-mediated phosphorylation of both ezrin and paxillin was detected by immunoblotting with Abs that specifically recognize the phosphorylated active forms of ezrin and paxillin (Fig. 8A). The above data indicate that the Stx1-B-mediated intracellular signal induces the phosphorylation of ezrin and paxillin during the course of cytoskeletal remodeling.

As shown in Fig. 8B, the effect of Stx1-B on the induction of ezrin phosphorylation is dose-dependent and the concentration of 1 μg/ml was found to be sufficient to yield maximum effect. As shown in Fig. 8C, we also found that the treatment with anti-Gb3 Abs similarly induces the phosphorylation of ezrin in ACHN cells. Therefore, the ligation of Gb3 by pentameric Stx1-B is not always required to induce cytoskeletal signaling and the binding of monomeric forms of the ligand to Gb3 might be able to induce ezrin phosphorylation.

We also examined whether constitutive Stx1-B treatment is required to induce ezrin phosphorylation. For this purpose, we bound Stx1-B to ACHN cells on ice and then removed excess toxin by washing, before shifting the temperature to 37°C. As shown in Fig. 8D, after the temperature was shifted to 37°C, transient increase in phosphorylation of ezrin was observed by immunoblotting. Although the elevation of ezrin phosphorylation observed in this experiment is slower than that presented in Fig. 8A, it is probably due to the time lag for warming up of the medium to 37°C after the temperature shift. These data indicate that the primary ligation of the plasma membrane Gb3 pool by Stx1-B is sufficient to induce intracellular signal for cytoskeletal rearrangements.

Effect of inhibitors on Stx1-B-induced cytoskeletal remodeling

To clarify the signaling cascade that induces the phosphorylation of ezrin, we examined the effect of a number of inhibitors on Stx1-B-induced ezrin phosphorylation. As shown in Fig. 9, when ACHN cells were pre-treated with PP2, a specific inhibitor for Src family PTK, the Stx1-B-mediated phosphorylation of ezrin was clearly inhibited. Similary, MBD, which is known to disturb the structure of the lipid rafts through the depletion of cholesterol from the cell membrane,

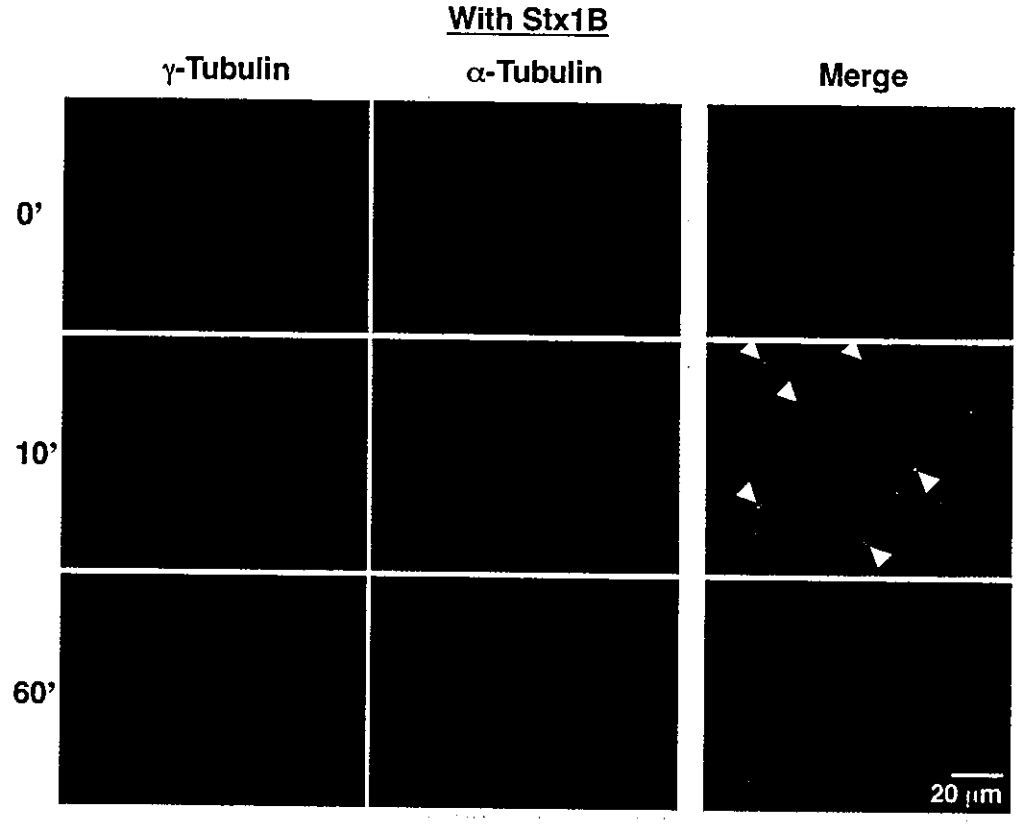

Fig. 6. Effect of Stx1-B subunit on the distribution of γ- and α-tubulins in ACHN cells. ACHN cells were examined as described in Fig. 2 using Alexa-488-labeled anti-γ-tubulin Ab (left panels, green) and Alexa-546-labeled anti-α-tubulin mAb (center panels, red). The arrowheads indicate the accumulation of γ-tubulin at the microtubule-organizing centers. Results are representative of three independent experiments.

inhibited the Stx1-B-mediated phosphorylation of ezrin (Fig. 9). In addition, LY294002, a specific inhibitor for PI3K, and Y27632, a specific inhibitor for ROCK, also inhibited the Stx1-B-mediated phosphorylation of ezrin (Fig. 9). In contrast, PKC inhibitor 20-28 (Fig. 9) and PKC inhibitor EGF-R fragment 651-658 (data not shown) did not affect the Stx1-B-mediated phosphorylation of ezrin in ACHN cells.

We next examined whether these inhibitors affect the Stx1-B-mediated cytoskeletal rearrangements. As shown in Fig. 2 and Fig. 10A, Stx1-B treatment induced the clustering of ezrin beneath the plasma membrane (indicated by arrowhead). When ACHN cells were pretreated with any of inihibitors, including PP2, MBD, LY294002 and Y27632, however, the Stx1-B-induced clustering of ezrin was not observed (Fig. 10A). Therefore, it is suggested that the inhibition of ezrin phosphorylation by these inhibitors suppresses Stx1-B-mediated redistribution of ezrin.

To clarify the molecule responsible for the redistribution of vimentin during the course of Stx1-B-induced cytoskeletal remodeling, we next examined the effect of inhibitors on the Stx1-B-induced redistribution of vimentin. As shown in Fig. 5 and Fig. 10B, Stx1-B treatment induced the accumulation of vimentin in the paranuclear area (indicated by arrowhead). When ACHN cells were pretreated with either PP2 or Y27632, however, the Stx1-B-induced clustering of vimentin in the paranuclear region was not observed (Fig. 10B), indicating the involvement of the Src family PTK and ROCK in the Stx1-B-mediated redistribution of vimentin.

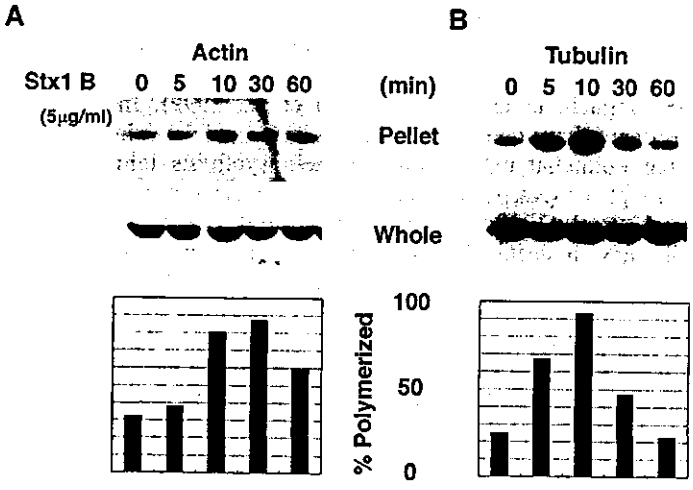

Fig. 7. Effect of Stx1-B subunit on the polymerization of actin and tubulin in ACHN cells. (A) ACHN cells were treated with and without 5 μg/ml of the Stx1-B subunit as described in Fig. 1 and lysed in the actin stabilization buffer. After removing aliquots from each whole lysate for the determination of total actin, polymerized actin (filamentous actin) was separated from soluble actin (monomer actin) by centrifugation. Both fractions of polymerized actin (pellet, upper panel) and total actin (whole, mid panel) were detected by immunoblot analysis and quantitated by densitometry. The proportion (%) polymerized was calculated by dividing the actin in the pellet fraction by the actin in the whole lysate and indicated (lower panel). (B) Tubulin polymerization was examined as in A.

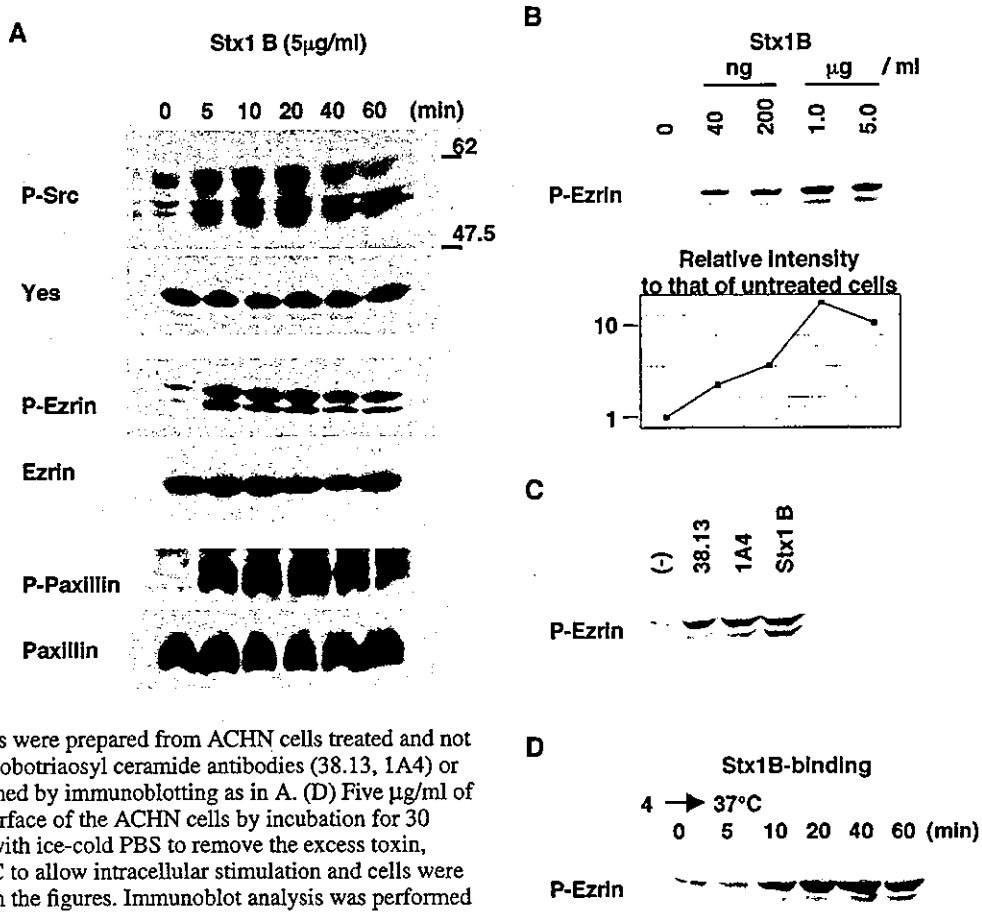

Fig. 8. Transient phosphorylation of ezrin in ACHN cells after treatment with the Stx1-B subunit. (A) Total cell extracts were prepared from ACHN cells treated with or without 5 μg/ml of Stx1-B subunit for the indicated periods. After separation on 10% SDS-PAGE gel, the proteins were transferred to a nitrocellulose membrane and immunoblotted using the indicated antibodies. (B) Total cell extracts were prepared from ACHN cells treated with or without different amounts of Stx1-B subunit for 10 minutes and immunoblot analysis was performed using anti-phospho-specific ezrin antibody (P-Ezrin) as in A. Intensity of the phospho-ezrin signals obtained from each sample was quantitated by densitometry and the relative value of each to that of untreated cells (each value/the value of untreated cells) was indicated as a graph (lower panel). (C) Total cell extracts were prepared from ACHN cells treated and not treated with 5 μg/ml each of either anti-globotriaosyl ceramide antibodies (38.13, 1A4) or Stx1-B subunit for 10 minutes and examined by immunoblotting as in A. (D) Five μg/ml of Stx1-B pentamer was bound to the cell surface of the ACHN cells by incubation for 30 minutes at 4°C. After intensive washing with ice-cold PBS to remove the excess toxin, temperature was shifted from 4°C to 37°C to allow intracellular stimulation and cells were incubated for the time periods indicated in the figures. Immunoblot analysis was performed as in A.

Discussion

In this report, we clearly demonstrated that the binding of Stx1-B induces intracellular signals that initiate cytoskeleton remodeling in ACHN renal carcinoma cells, which are related to renal tubular epithelial cells. These signals led to morphological changes and a weakened adhesiveness of the cells. The series of cellular and biological events induced by Stx1-B binding was similar to that which occurs during the course of growth factor-stimulated cell motility (Bretscher, 1989; Leventhal et al., 1997).

Several lines of evidence, including our own, have suggested that Stx directly injures renal tubular epithelial cells. For example, renal tubular epithelial cells express Gb3, which can bind Stx1 and 2 (Boyd and Lingwood, 1989; Kiyokawa et al., 1998; Taguchi et al., 1998; Uchida et al., 1999). In vitro experiments have revealed that Stx1 induces cell death in renal tubular epithelial cells through protein synthesis inhibition and apoptosis (Karpman et al., 1998; Kiyokawa et al., 1998; Taguchi et al., 1998; Williams et al., 1999). Several clinical studies have indicated the involvement of renal tubular damage during the course of HUS (Kaneko et al., 2001; Takeda et al., 1993). The appearance of apoptotic cells in the renal tubules of the kidney in HUS patients, accompanied by STEC infection, further indicates that renal tubular injury does occur in the kidneys of HUS patients (Karpman et al., 1998; Taguchi et al., 1998).

The essential cytotoxicity of Stx is generally thought to arise from the inhibition of protein synthesis by the Stx-A subunit. However, recent studies have shown that the B-subunit also has biological effects on target cells through a mechanism mediated by intracellular signals upon binding to Gb3 (Katagiri et al., 1999; Kiyokawa et al., 2001; Mangeney et al., 1993; Mori et al., 2000; Taga et al., 1997). Although Stx1-B-induced intracellular signals are known to mediate apoptosis in Burkitt's lymphoma cells, their biological effect on other cell species has not been clarified. The data presented in this study extend previous observations and indicate that Stx1-B-induced intracellular signals induce cytoskeleton remodeling, resulting in morphological changes in the target cells. As previously reported, the simultaneous addition of Stx1-B subunits enhances the cytotoxic effect of Stx1 holotoxins on ACHN cells, suggesting a synergism between A-subunit-mediated protein synthesis inhibition and B-subunit-mediated intracellular signals on the cytotoxicity observed in target cells (Katagiri et al., 2001). Although the biological significance of Stx1-B-induced cytoskeletal remodeling in target cells in vivo is not presently known, this process might participate in Stx-induced cell injury, thereby playing a role in the development of complications associated with STEC infection, such as HUS.

Gb3 acts as functional receptor for Stx, but the natural ligand of this lipid and its normal physiological role are unknown. Upon binding with its natural ligand, Gb3 might mediate intracellular signals leading to cytoskeletal remodeling,

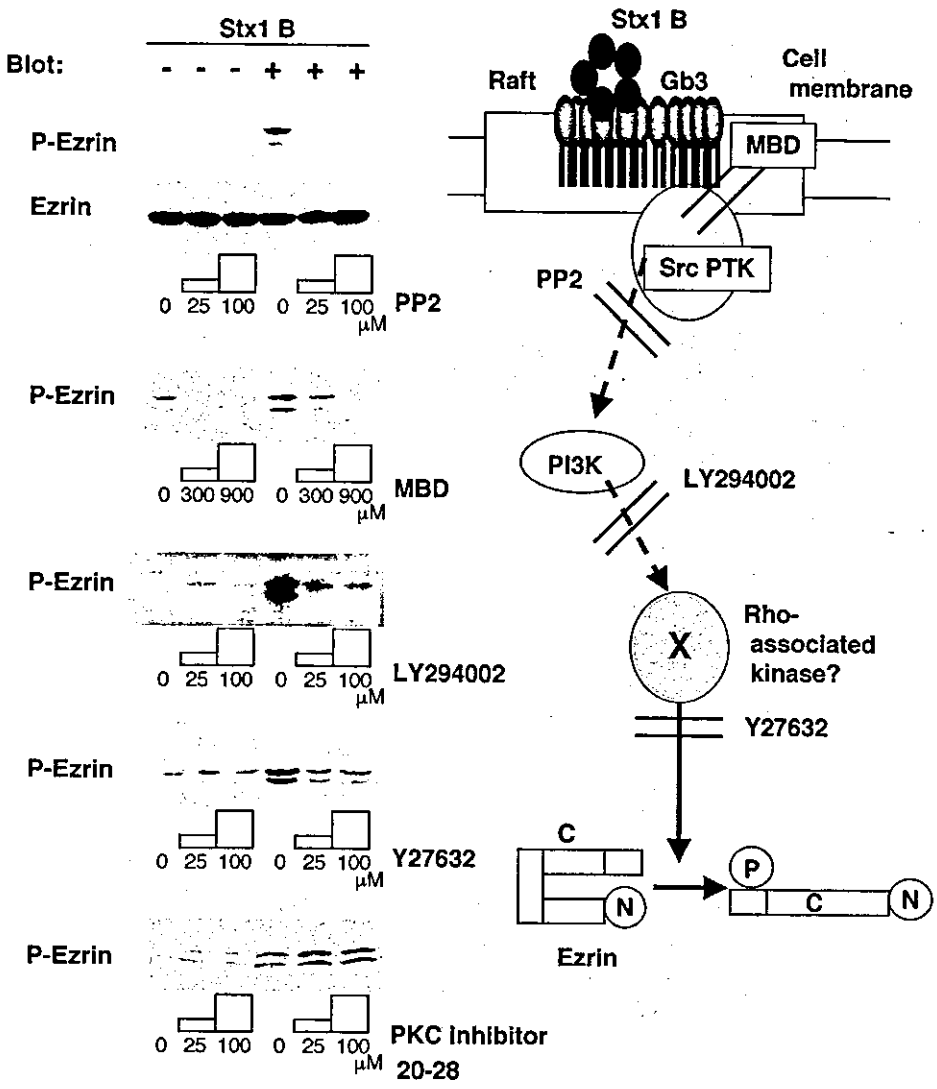

Fig. 9. Effect of inhibitors on the Stx1-B-subunit-mediated phosphorylation of ezrin. ACHN cells were preincubated with the inhibitors shown in the figure for three hours. The concentrations of 300 and 900 μM for MBD and 25 and 100 μM for other inhibitors were used. After treatment with the Stx1-B subunit for 5 minutes, cell extracts were prepared, and immunoblotting for phospho-specific ezrin was performed as described in Fig. 8. In parallel, each sample was examined using an anti-ezrin antibody to confirm that the protein amounts in each lane were comparable (only the result for PP2 is shown in the second panel from the top). In the right panel, the effect of each inhibitor is schematically presented.

participating in the development and organization of kidney tissue. Therefore, our observation might provide an in vitro model for research on lipid-receptor-mediated signaling systems for cytoskeletal remodeling.

Stx1-B binding induces the phosphorylation of ezrin, a linker protein that connects the plasma membrane and the actin cytoskeleton and is involved in cell adhesion and the formation of the free-surface domain of plasma membranes, especially in the ruffling and organization of microvilli (Berryman et al., 1995; Bretscher et al., 1997; Chen et al., 1995; Crepadi et al., 1997; Kondo et al., 1997; Takeuchi et al., 1994; Tsukita and Yonemura, 1999). Stx1-B-induced ezrin phosphorylation was inhibited both by MBD (which disturbs the structure of lipid rafts) and by the Src family PTK inihibitor PP2. Furthermore, we previously reported that Gb3 is mainly located on lipid rafts in the cell membrane, and that Stx1-B binding to Gb3 induces a clustering of the lipid rafts, leading to the activation of Src family PTK (which is anchored to the inner layer of the lipid rafts) possibly by aggregation-mediated kinase auto-phosphorylation (Katagiri et al., 1999; Mori et al., 2000). Thus, our data indicate that the lipid-raft-mediated activation of Src family PTK might play an important role in the phosphorylation of ezrin during the course of Stx-induced cytoskeleton remodeling. In addition to MBD and PP2, we also found that the inhibition of both PI3K and ROCK by their specific inhibitors abolished the Stx1-B-mediated phosphorylation of ezrin, suggesting that these molecules are located downstream from Src family PTK in the signaling cascade and participate in the Stx1-B-mediated phosphorylation of ezrin.

Several molecules have been postulated to be responsible for the phosphorylation of ezrin. For example, the Ras superfamily small G-proteins Rho, Rac and Cdc42 have been shown to be responsible for the formation of focal contact, lamellipodia and filopodia, respectively (Van Aelst and D'Souza-Schorey, 1997; Mackay and Hall, 1998). During these processes, the ERM proteins are thought to be located downstream of the small G-proteins (Bretscher et al., 1997; Matsui et al., 1998; Shaw et al., 1998; Tsukita and Yonemura, 1999). Furthermore, it has been shown that ROCK phosphorylates the C-terminal threonines of ERM proteins, regulating their head-to-tail association in in vitro experiments (Matsui et al., 1998).

We also know that myotonic dystrophy kinase-related Cdc42-binding kinase (MRCK) is a candidate for the kinase that phosphorylates ERM proteins at filopodia (Nakamura et al., 2000). In the case of Merlin, which is closely related to the ERM proteins, p21-activated kinase 2 (PAK2), a downstream effector of Rac and Cdc42, has been postulated as a candidate for the kinase that phosphorylates this protein (Kissil et al., 2002). Consistent with the above observations, we report here that the ROCK inhibitor Y27632 inhibited the Stx1-B-stimulated phosphorylation of ezrin, suggesting that ROCK is at least one of the kinases responsible for ezrin phosphorylation in Stx1-B-induced cytoskeletal remodeling. In addition, Rac and Cdc42 might also be involved in the process, as Stx1-B stimulation induces the extension of lamellipodia- and

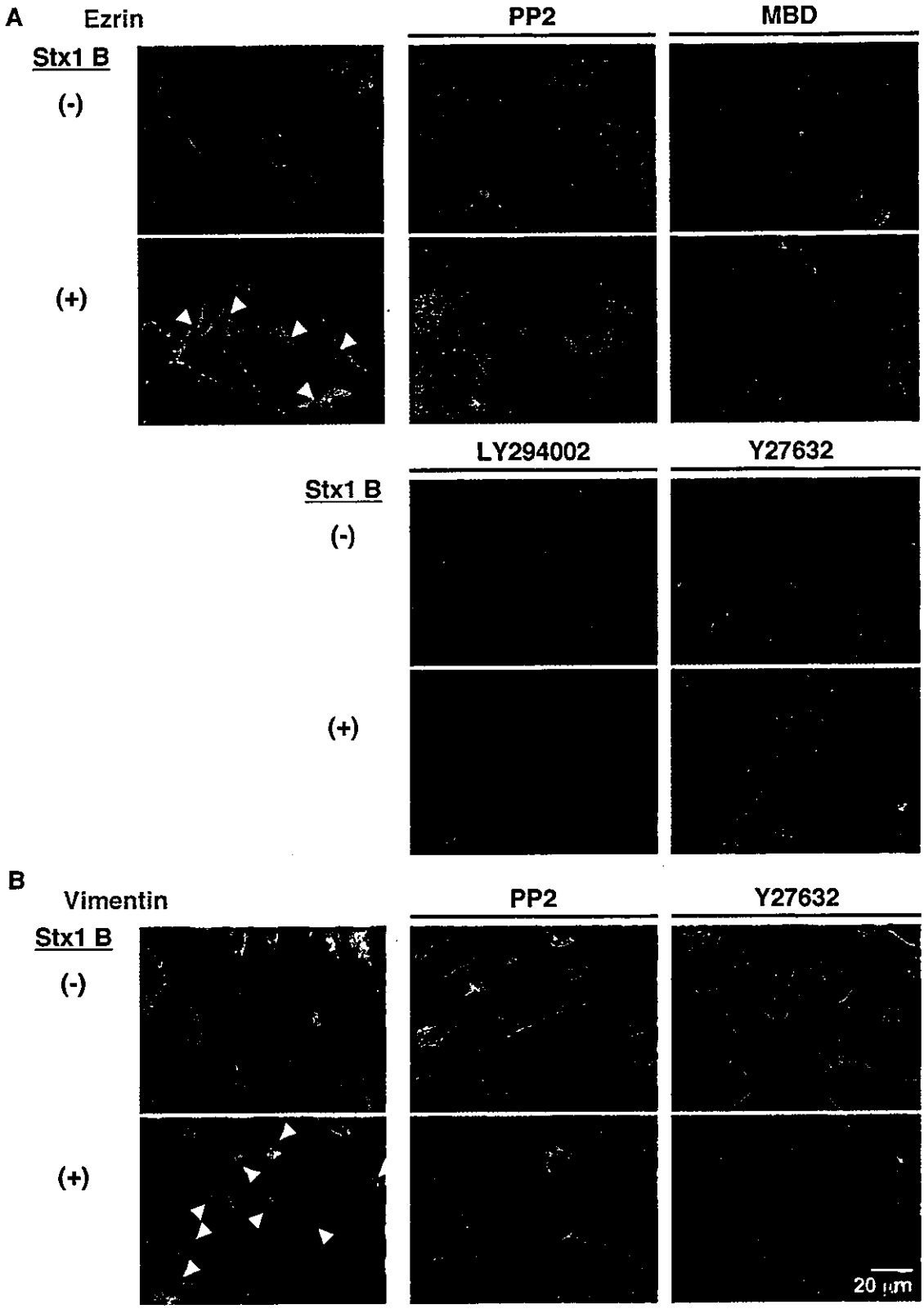

Fig. 10. Effect of inhibitors on the Stx1-B-subunit-mediated clustering of ezrin and vimentin. (A) ACHN cells were preincubated with the inhibitors shown in the figure for three hours. The concentrations of 900 μM for MBD and 100 μM for other inhibitors were used. After treatment with the Stx1-B subunit for 10 minutes, the cells were fixed and stained with anti-ezrin monoclonal antibody (green) followed by counterstaining with DAPI (blue) as in Fig. 2. Results are representative of three independent experiments. The clustering of ezrin was indicated by arrowhead. (B) ACHN cells pre-incubated with inhibitors as in A were treated with the Stx1-B for 30 minutes and stained with anti-vimentin monoclonal antibody (green) as in A.

filopodia-like structures. Further experiments investigating the involvement of small G-proteins and their downstream kinases in the Stx1-B-induced signaling system of cytoskeletal remodeling are now underway.

Conversely, it has been suggested that ezrin was a downstream effector of PKCα during the course of integrin-mediated cell migration (Ng et al., 2001). PKCθ is a major kinase specific for moesin, a family protein of ezrin (Pietromonaco et al., 1998). PKCθ is involved in regulating the localization and association of CD44 and ezrin during cell motility and invasion (Legg et al., 2002; Stapleton et al., 2002). As shown in this study, however, the PKC-inhibitors did not affect the Stx1-B-stimulated phosphorylation of ezrin. Our data might indicate that PKCs are not essential for the Stx1-B-induced phosphorylation of ezrin in our experimental system.

In addition to the phosphorylation of ezrin, we also observed changes in the distributions of several molecules, including FAK, paxillin, vimentin, cytokeratin and tubulins, all of which contribute to the organization of the cytosleleton. The molecular mechanism responsible for the above-described redistribution of cytoskeletal molecules has not yet been clarified. However, as observed in the present study, treatment with the ROCK inhibitor Y27632 abolished the Stx1-B-stimulated relocalization of vimentin, suggesting the involvement of ROCK in the Stx1-B-induced redistribution of vimentin. The ability of ROCK to phosphorylate vimentin in vitro and in vivo (Goto et al., 1998; Kosako et al., 1999) might support this idea.

In conclusion, Stx1-B-induced intracellular signals mediate the remodeling of a variety of cytoskeletal organizing proteins, resulting in changes in cell morphology. Although additional studies are clearly necessary, further investigation of the mechanism of Stx1-B-mediated cytoskeletal remodeling should provide an in vitro model for future research on the pathogenesis of Stx-mediated cell injury as well as the role of lipid raft-mediated cell signaling in cytoskeletal remodeling.

This work was supported in part by Health and Labour Sciences Research Grants from the Ministry of Health, Labour and Welfare of Japan and MEXT. KAKENHI 15019129, JSPS. KAKENHI 15390133 and 15590361. This work was also supported by a grant from the Japan Health Sciences Foundation for Research on Health Sciences Focusing on Drug Innovation. Additional support was provided by a grant from Sankyo Foundation of Life Science. We thank M. Sone and S. Yamauchi for their excellent secretarial works. We thank S. Hakomori and Otsuka Assay Laboratories for gifting anti-Gb3 mAb 1A4.

References

Andreoli, C., Martin, M., le Borgne, R., Reggio, H. and Mangeat, P. (1994). Ezrin has properties to self-associate at the plasma membrane. *J. Cell Sci.* **107**, 2509-2521.

Arpin, M., Algrain, M. and Louvard, D. (1994). Membrane-actin microfilament connections: an increasing diversity of players related to band 4.1. *Curr. Opin. Cell Biol.* **6**, 136-141.

Berryman, M., Gary, R. and Bretscher, A. (1995). Ezrin oligomers are major cytoskeletal components of placental microvilli: a proposal for their involvement in cortical morphogenesis. *J. Cell Biol.* **131**, 1231-1242.

Boyd, B. and Lingwood, C. (1989). Verotoxin receptor glycolipid in human renal tissue. *Nephron* **51**, 207-210.

Bretscher, A. (1989). Rapid phosphorylation and reorganization of ezrin and spectrin accompany morphological changes induced in A-431 cells by epidermal growth factor. *J. Cell Biol.* **108**, 921-930.

Bretscher, A., Gary, R. and Berryman, M. (1995). Soluble ezrin purified from placenta exists as stable monomers and elongated dimers with masked C-terminal ezrin-radixin-moesin association domains. *Biochemistry* **34**, 16830-16837.

Bretscher, A., Reczek, D. and Berryman, M. (1997). Ezrin: a protein requiring conformational activation to link microfilaments to the plasma membrane in the assembly of cell surface structures. *J. Cell Sci.* **110**, 3011-3018.

Burridge, K., Turner, C. E. and Romer, L. H. (1992). Tyrosine phosphorylation of paxillin and pp125FAK accompanies cell adhesion to extracellular matrix: a role in cytoskeletal assembly. *J. Cell Biol.* **119**, 893-903.

Chen, J., Cohn, J. A. and Mandel, L. J. (1995). Dephosphorylation of ezrin as an early event in renal microvillar breakdown and anoxic injury. *Proc. Natl. Acad. Sci. USA* **92**, 7495-7499.

Crepaldi, T., Gautreau, A., Comoglio, P. M., Louvard, D. and Arpin, M. (1997). Ezrin is an effector of hepatocyte growth factor-mediated migration and morphogenesis in epithelial cells. *J. Cell Biol.* **138**, 423-434.

Glogauer, M., Arora, P., Yao, G., Sokholov, I., Ferrier, J. and McCulloch, C. A. (1997). Calcium ions and tyrosine phosphorylation interact coordinately with actin to regulate cytoprotective responses to stretching. *J. Cell Sci.* **110**, 11-21.

Goto, H., Kosako, H., Tanabe, K., Yanagida, M., Sakurai, M., Amano, M., Kaibuchi, K. and Inagaki, M. (1998). Phosphorylation of vimentin by Rho-associated kinase at a unique amino-terminal site that is specifically phosphorylated during cytokinesis. *J. Biol. Chem.* **273**, 11728-11736.

Heacock, C. S. and Bamburg, J. R. (1983). The quantification of G- and F-actin in cultured cells. *Anal. Biochem.* **135**, 22-36.

Heiska, L., Alfthan, K., Gronholm, M., Vilja, P., Vaheri, A. and Carpen, O. (1998). Association of ezrin with intercellular adhesion molecule-1 and -2 (ICAM-1 and ICAM-2). Regulation by phosphatidylinositol 4, 5-bisphosphate. *J. Biol. Chem.* **273**, 21893-21900.

Hirao, M., Sato, N., Kondo, T., Yonemura, S., Monden, M., Sasaki, T., Takai, Y., Tsukita, S. and Tsukita, S. (1996). Regulation mechanism of ERM (ezrin/radixin/moesin) protein/plasma membrane association: possible involvement of phosphatidylinositol turnover and Rho-dependent signaling pathway. *J. Cell Biol.* **135**, 37-51.

Kaneko, K., Kiyokawa, N., Ohtomo, Y., Nagaoka, R., Yamashiro, Y., Taguchi, T., Mori, T., Fujimoto, J. and Takeda, T. (2001). Apoptosis of renal tubular cells in Shiga-toxin-mediated hemolytic uremic syndrome. *Nephron* **87**, 182-185.

Kaplan, B. S., Cleary, T. G. and Obrig, T. G. (1990). Recent advances in understanding the pathogenesis of the hemolytic uremic syndromes. *Pediatr. Nephrol.* **4**, 276-283.

Karpman, D., Hakansson, A., Perez, M. T., Isaksson, C., Carlemalm, E., Caprioli, A. and Svanborg, C. (1998). Apoptosis of renal cortical cells in the hemolytic-uremic syndrome: in vivo and in vitro studies. *Infect. Immun.* **66**, 636-644.

Katagiri, U. Y., Mori, T., Nakajima, H., Katagiri, C., Taguchi, T., Takeda, T., Kiyokawa, N. and Fujimoto, J. (1999). Activation of Src family kinase Yes induced by Shiga toxin binding to globotriaosyl ceramide (Gb3/CD77) in low density, detergent-insoluble microdomains. *J. Biol. Chem.* **274**, 35278-35282.

Katagiri, U. Y., Kiyokawa, N. and Fujimoto, J. (2001). The effect of Shiga toxin binding to globotriaosylceramide in rafts of human kidney cells and Burkitt's lymphomaa cells. *Trends. Glycosci. Glycotech.* **13**, 281-290.

Kissil, J. L., Johnson, K. C., Eckman, M. S. and Jacks, T. (2002). Merlin phosphorylation by p21-activated kinase 2 and effects of phosphorylation on merlin localization. *J. Biol. Chem.* **277**, 10394-10399.

Kiyokawa, N., Taguchi, T., Mori, T., Uchida, H., Sato, N., Takeda, T. and Fujimoto, J. (1998). Induction of apoptosis in normal human renal tubular epithelial cells by *Escherichia coli* Shiga toxins 1 and 2. *J. Infect. Dis.* **178**, 178-184.

Kiyokawa, N., Mori, T., Taguchi, T., Saito, M., Mimori, K., Suzuki, T., Sekino, T., Sato, N., Nakajima, H., Katagiri, Y. U. et al. (2001). Activation of the caspase cascade during Stx1-induced apoptosis in Burkitt's lymphoma cells. *J. Cell. Biochem.* **81**, 128-142.

Knowles, G. C. and McCulloch, C. A. (1992). Simultaneous localization and quantification of relative G and F actin content: optimization of fluorescence labeling methods. *J. Histochem. Cytochem.* **40**, 1605-1612.

Kojio, S., Zhang, H., Ohmura, M., Gondaira, F., Kobayashi, N. and Yamamoto, T. (2000). Caspase-3 activation and apoptosis induction coupled with the retrograde transport of shiga toxin: inhibition by brefeldin A. *FEMS Immunol. Med. Microbiol.* **29**, 275-281.

Kondo, T., Takeuchi, K., Doi, Y., Yonemura, S., Nagata, S. and Tsukita, S. (1997). ERM (ezrin/radixin/moesin)-based molecular mechanism of microvillar breakdown at an early stage of apoptosis. *J. Cell Biol.* **139**, 749-758.

Kosako, H., Goto, H., Yanagida, M., Matsuzawa, K., Fujita, M., Tomono, Y., Okigaki, T., Odai, H., Kaibuchi, K. and Inagaki, M. (1999). Specific accumulation of Rho-associated kinase at the cleavage furrow during cytokinesis: cleavage furrow-specific phosphorylation of intermediate filaments. *Oncogene* **18**, 2783-2788.

Legg, J. W., Lewis, C. A., Parsons, M., Ng, T. and Isacke, C. M. (2002). A novel PKC-regulated mechanism controls CD44 ezrin association and directional cell motility. *Nat. Cell Biol.* **4**, 399-407.

Leventhal, P. S., Shelden, E. A., Kim, B. and Feldman, E. L. (1997). Tyrosine phosphorylation of paxillin and focal adhesion kinase during insulin-like growth factor-I-stimulated lamellipodial advance. *J. Biol. Chem.* **272**, 5214-5218.

Lingwood, C. A. (1996). Role of verotoxin receptors in pathogenesis. *Trends Microbiol.* **4**, 147-153.

Mackay, D. J. and Hall, A. (1998). Rho GTPases. *J. Biol. Chem.* **273**, 20685-20688.

Mangeney, M., Lingwood, C. A., Taga, S., Caillou, B., Tursz, T. and Wiels, J. (1993). Apoptosis induced in Burkitt's lymphoma cells via Gb3/CD77, a glycolipid antigen. *Cancer Res.* **53**, 5314-5319.

Matsui, T., Maeda, M., Doi, Y., Yonemura, S., Amano, M., Kaibuchi, K., Tsukita, S. and Tsukita, S. (1998). Rho-kinase phosphorylates COOH-terminal threonines of ezrin/radixin/moesin (ERM) proteins and regulates their head-to-tail association. *J. Cell Biol.* **140**, 647-657.

McCormack, S. A., Ray, R. M., Blanner, P. M. and Johnson, L. R. (1999). Polyamine depletion alters the relationship of F-actin, G-actin, and thymosin beta4 in migrating IEC-6 cells. *Am. J. Physiol.* **276**, C459-C468.

Minotti, A. M., Barlow, S. B. and Cabral, F. (1991). Resistance to antimitotic drugs in Chinese hamster ovary cells correlates with changes in the level of polymerized tubulin. *J. Biol. Chem.* **266**, 3987-3994.

Montgomery, R. B., Guzman, J., O'Rourke, D. M. and Stahl, W. L. (2000). Expression of oncogenic epidermal growth factor receptor family kinases induces paclitaxel resistance and alters beta-tubulin isotype expression. *J. Biol. Chem.* **275**, 17358-17363.

Mori, T., Kiyokawa, N., Katagiri, Y. U., Taguchi, T., Suzuki, T., Sekino, T., Sato, N., Ohmi, K., Nakajima, H., Takeda, T. et al. (2000). Globotriaosyl ceramide (CD77/Gb3) in the glycolipid-enriched membrane domain participates in B-cell receptor-mediated apoptosis by regulating lyn kinase activity in human B cells. *Exp. Hematol.* **28**, 1260-1268.

Moritz, M. and Agard, D. A. (2001). γ-tubulin complexes and microtubule nucleation. *Curr. Opin. Struct. Biol.* **11**, 174-181.

Nakajima, H., Katagiri, Y. U., Kiyokawa, N., Taguchi, T., Suzuki, T., Sekino, T., Mimori, K., Saito, M., Nakao, H., Takeda, T. et al. (2001). Single-step method for purification of Shiga toxin-1 B subunit using receptor-mediated affinity chromatography by globotriaosylceramide-conjugated octyl sepharose CL-4B. *Protein Expr. Purif.* **22**, 267-275.

Nakamura, N., Oshiro, N., Fukata, Y., Amano, M., Fukata, M., Kuroda, S., Matsuura, Y., Leung, T., Lim, L. and Kaibuchi, K. (2000). Phosphorylation of ERM proteins at filopodia induced by Cdc42. *Gene. Cell.* **5**, 571-581.

Ng, T., Parsons, M., Hughes, W. E., Monypenny, J., Zicha, D., Gautreau, A., Arpin, M., Gschmeissner, S., Verveer, P. J., Bastiaens, P. I. et al. (2001). Ezrin is a downstream effector of trafficking PKC-integrin complexes involved in the control of cell motility. *EMBO J.* **20**, 2723-2741.

Pietromonaco, S. F., Simons, P. C., Altman, A. and Elias, L. (1998). Protein kinase C-theta phosphorylation of moesin in the actin-binding sequence. *J. Biol. Chem.* **273**, 7594-7603.

Richardson, S. E., Karmali, M. A., Becker, L. E. and Smith, C. R. (1988). The histopathology of the hemolytic uremic syndrome associated with verocytotoxin-producing *Escherichia coli* infections. *Hum. Pathol.* **19**, 1102-1108.

Rodgers, W. and Rose, J. K. (1996). Exclusion of CD45 inhibits activity of p56lck associated with glycolipid-enriched membrane domains. *J. Cell Biol.* **135**, 1515-1523.

Serrador, J. M., Alonso-Lebrero, J. L., del Pozo, M. A., Furthmayr, H., Schwartz-Albiez, R., Calvo, J., Lozano, F. and Sanchez-Madrid, F. (1997). Moesin interacts with the cytoplasmic region of intercellular adhesion molecule-3 and is redistributed to the uropod of T lymphocytes during cell polarization. *J. Cell Biol.* **138**, 1409-1423.

Shaw, R. J., Henry, M., Solomon, F. and Jacks, T. (1998). RhoA-dependent phosphorylation and relocalization of ERM proteins into apical membrane/actin protrusions in fibroblasts. *Mol. Biol. Cell* **9**, 403-419.

Simons, K. and Ikonen, E. (1997). Functional rafts in cell membranes. *Nature* **387**, 569-572.

Stapleton, G., Malliri, A. and Ozanne, B. W. (2002). Downregulated AP-1 activity is associated with inhibition of protein-kinase-C-dependent CD44 and ezrin localisation and upregulation of PKC theta in A431 cells. *J. Cell Sci.* **115**, 2713-2724.

Taga, S., Carlier, K., Mishal, Z., Capoulade, C., Mangeney, M., Lecluse, Y., Coulaud, D., Tetaud, C., Pritchard, L. L., Tursz, T. et al. (1997). Intracellular signaling events in CD77-mediated apoptosis of Burkitt's lymphoma cells. *Blood* **90**, 2757-2767.

Taguchi, T., Uchida, H., Kiyokawa, N., Mori, T., Sato, N., Horie, H., Takeda, T. and Fujimoto, J. (1998). Verotoxins induce apoptosis in human renal tubular epithelium derived cells. *Kidney Int.* **53**, 1681-1688.

Takeda, T., Dohi, S., Igarashi, T., Yamanaka, T., Yoshiya, K. and Kobayashi, N. (1993). Impairment by verotoxin of tubular function contributes to the renal damage seen in haemolytic uraemic syndrome. *J. Infect.* **27**, 339-341.

Takeuchi, K., Sato, N., Kasahara, H., Funayama, N., Nagafuchi, A., Yonemura, S., Tsukita, S. and Tsukita, S. (1994). Perturbation of cell adhesion and microvilli formation by antisense oligonucleotides to ERM family members. *J. Cell Biol.* **125**, 1371-1384.

Tsukita, S. and Yonemura, S. (1997). ERM (ezrin/radixin/moesin) family: from cytoskeleton to signal transduction. *Curr. Opin. Cell Biol.* **9**, 70-75.

Tsukita, S. and Yonemura, S. (1999). Cortical actin organization: lessons from ERM (ezrin/radixin/moesin) proteins. *J. Biol. Chem.* **274**, 34507-34510.

Tsukita, S., Oishi, K., Sato, N., Sagara, J., Kawai, A. and Tsukita, S. (1994). ERM family members as molecular linkers between the cell surface glycoprotein CD44 and actin-based cytoskeletons. *J. Cell Biol.* **126**, 391-401.

Tsukita, S., Yonemura, S. and Tsukita, S. (1997). ERM proteins: head-to-tail regulation of actin-plasma membrane interaction. *Trends. Biochem. Sci.* **22**, 53-58.

Turunen, O., Wahlstrom, T. and Vaheri, A. (1994). Ezrin has a COOH-terminal actin-binding site that is conserved in the ezrin protein family. *J. Cell Biol.* **126**, 1445-1453.

Uchida, H., Kiyokawa, N., Horie, H., Fujimoto, J. and Takeda, T. (1999). The detection of Shiga toxins in the kidney of a patient with hemolytic uremic syndrome. *Pediatr. Res.* **45**, 133-137.

Van Aelst, L. and D'Souza-Schorey, C. (1997). Rho GTPases and signaling networks. *Genes. Dev.* **11**, 2295-2322.

Williams, J. M., Lea, N., Lord, J. M., Roberts, L. M., Milford, D. V. and Taylor, C. M. (1997). Comparison of ribosome-inactivating proteins in the induction of apoptosis. *Toxicol. Lett.* **91**, 121-127.

Williams, J. M., Boyd, B., Nutikka, A., Lingwood, C. A., Barnett-Foster, D. E., Milford, D. V. and Taylor, C. M. (1999). A comparison of the effects of verocytotoxin-1 on primary human renal cell cultures. *Toxicol. Lett.* **105**, 47-57.

Yonemura, S., Nagafuchi, A., Sato, N. and Tsukita, S. (1993). Concentration of an integral membrane protein, CD43 (leukosialin, sialophorin), in the cleavage furrow through the interaction of its cytoplasmic domain with actin-based cytoskeletons. *J. Cell Biol.* **120**, 437-449.

Microbiol. Immunol., 48(5), 377–387, 2004

Characterization of a Shiga-Toxin 1-Resistant Stock of Vero Cells

Takaomi Sekino[1,*], Nobutaka Kiyokawa[*,1], Tomoko Taguchi[1], Hisami Takenouchi[1], Jun Matsui[1], Wei-Ran Tang[1], Toyo Suzuki[1], Hideki Nakajima[1], Masahiro Saito[1], Kazuhiro Ohmi[1], Yohko U. Katagiri[1], Hajime Okita[1], Hiroshi Nakao[2], Tae Takeda[3,†], and Junichiro Fujimoto[1]

[1]*Department of Developmental Biology, National Research Institute for Child Health and Development, Setagaya-ku, Tokyo 154–8567, Japan,* [2]*Faculty of Pharmaceutical Sciences, Okayama University, Okayama, Okayama 700–8530, Japan, and* [3]*Department of Infectious Diseases Research, National Children's Medical Research Center, Setagaya-ku, Tokyo 154–8567, Japan*

Received November 5, 2003; in revised form, January 26, 2004. Accepted February 16, 2004

Abstract: **Shiga toxins (Stxs, also referred to as verotoxins) were first described as a novel cytotoxic activity against Vero cells. In this study, we report the characterization of an Stx1-resistant (R-) stock of Vero cells. (1) When the susceptibility of R-Vero cells to Stx1 cytotoxicity was compared to that of Stx1-sensitive (S-) Vero cells by methylthiazolyldiphenyl-tetrazolium bromide (MTT) assay, cell viability after 48-hr exposure to 10 pg/ml of Stx1 was greater than 80% and less than 15%, respectively. (2) Although both a binding assay of fluorescence-labeled Stx1 and lipid analysis indicated considerable expression of Gb3Cer, a functional receptor for Stxs, in both Vero cells, anti-Gb3Cer monoclonal antibodies capable of binding to S-Vero cells failed to effectively label R-Vero cells, suggesting a conformational difference in the Gb3Cer expressed on R-Vero cells. (3) The lipid analysis also showed that the R-Vero cells contained significant amounts of Gb4Cer. In addition, introduction of exogenous Gb4Cer into S-Vero cells slightly inhibited Stx1 cytotoxicity, suggesting some correlation between glycosphingolipid composition and Stx1 resistance. (4) Both butyrate treatment and serum depression eliminated the Stx1 resistance of R-Vero cells. (5) The results of the analysis by confocal microscopy suggest a difference in intracellular transport of Stx1 between R-Vero and S-Vero cells. Further study of R-Vero cells may provide a model of Stx1 resistance via distinct intracellular transport of Stx1.**

Key words: **Shiga toxin, Vero cells, Toxin-resistant, Globotriaocyl ceramide**

Shiga toxin (Stx) is a family of protein toxins produced by Stx-producing strains of *Escherichia coli* (STEC), such as O157:H7, and it has been postulated to be the major cause of the development of serious complications associated with STEC infection, including hemolytic uremic syndrome (7, 29). Stx consists of two major types, Stx1 and Stx2. Stx1 differs from the Stx of *Shigella dysenteriae* type1 by a single amino acid in the A-subunit (15), while the amino acids of Stx2 are approximately 55% homologous with those of Stx1 (19).

All of these toxins are complexes of proteins consisting of two components, an A-subunit monomer and a B-subunit pentamer (17). The A subunit is a 30-kDa cytotoxic chain that possesses RNA *N*-glycohydrolase activity and cleaves a specific adenine residue on the 28S ribosomal RNA, resulting in inhibition of protein synthesis (17). By contrast, the 7-kDa B-subunit possesses the ability to bind with high affinity to the terminal digalactose of globotriaosyl ceramide (Gb3Cer), the functional receptor for Stx found on the specific types of the cells (17). Although Stx cytotoxicity is thought to

Address correspondence to Dr. Nobutaka Kiyokawa, Department of Developmental Biology, National Research Institute for Child Health and Development, 3–35–31 Taishido, Setagaya-ku, Tokyo 154–8567, Japan. Fax: +81–3–3487–9669. E-mail address: nkiyokawa@nch.go.jp

*Present address: Department of Pediatrics, University of Yamaguchi School of Medicine, Yamaguchi, Yamaguchi, Japan.

†Tae Takeda, M.D. & Ph. D. Died on May 15, 2001.

Abbreviations: Ab, antibody; FITC, fluorescein isothiocyanate; Gb3Cer, globotriaosyl ceramide; Gb4Cer, globotetraosyl ceramide; MTT, methylthiazolyldiphenyl-tetrazolium bromide; PBS, phosphate buffered saline; R-, resistant; S-, sensitive; STEC, Shiga-toxin-producing strains of *Escherichia coli*; Stx, Shiga toxin.

arise from the A-subunit that mediates the inhibition of protein synthesis, Stx must first bind to Gb3Cer on the target cell surface via its B-subunit, undergo endocytosis and be translocated to the cytosol to exert its cytotoxic effect.

Upon binding to Gb3Cer on the cell surface, Stx is aggregated into clathrine-coated pits and endocytosed (17, 32). After internalization, a portion of the internalized Stx molecules is delivered to the trans-Golgi network. Retrograde transport then carries the Stx molecules through the Golgi cisterns all the way to the endoplasmic reticulum, where the translocation of the A-subunit to the cytosol occurs (3, 17, 32). There, the Stx A-subunit displays its cytotoxicity by initiating RNA cleavage, thereby inhibiting protein synthesis. However, the existence of an alternate route of toxin transport to the lysosomes for degradation has also been reported (32).

Thus, the cytotoxicity of Stx is highly selective toward specific types of cells that express Gb3Cer, and, for example, it is widely believed that endothelial cells that express Gb3Cer are the main targets of Stx cytotoxicity in STEC infection (10, 23, 24, 36). In addition, renal tubular epithelial cells (5, 8, 12), mesangial cells (33, 40), macrophages/monocytes (37, 39), and neuronal cells (20, 30), all of which express Gb3Cer, have also been found to be directly affected by Stx. In addition to normal cells, a number of cell lines have been reported to be sensitive to Stx cytotoxicity. For example, the reason Stx is also called verotoxin is that it was first discovered as a novel cytotoxin toward Vero cells, which were derived from the kidneys of African green monkeys and express Gb3Cer (14). Burkitt's cell lines, such as Daudi (18) and renal-carcinoma-derived ACHN cells (34, 35), have also been reported to express Gb3Cer and to be highly sensitive to Stx.

However, several previous reports have revealed the existence of subclones of these cell lines that are resistant to Stx cytotoxicity. For example, Kongmuang et al. reported isolation of Stx-resistant Vero cells by treating them with nitrosoguanidine (13). Pudymaitis et al. also reported isolation of subclones of Daudi and Vero cells both of which are resistant for Stx (28). In each case, the mechanism of the toxin resistance has been explained by the lack of the Stx receptor Gb3Cer and the consequent inability of Stx to bind to the cells. In this paper, we report an Stx1-resistant stock of Vero cells that express Gb3Cer. Although Stx1 surely binds and is incorporated into the cells, significant resistance to cell death was observed in this stock. Further investigation the mechanism of resistance of the cells to Stx1 should help better understand the molecular mechanism of the cytotoxic action of Stx1 and provide a new approach to the prevention and treatment of Stx1 cytotoxicity during STEC infection.

Materials and Methods

Materials and cell culture. In this study, two different stocks of Vero cells, the one stored in the Department of Infectious Diseases Research, National Children's Medical Research Center, and the stock newly distributed by the Institute for Fermentation (Osaka, Japan), were used. An epidermoid carcinoma cell line A431 was obtained from the Japanese Cancer Research Resources Bank (Tokyo). Cells were cultured at 37 C in Dulbecco's Modified Eagle Medium supplemented with 10% fetal calf serum under a humidified 5% CO_2 atmosphere.

Stx1 was prepared as described previously (22) and distributed by Seikagaku Co. (Tokyo). The pentamer recombinant B-subunit of Stx1 was prepared as described previously (21). Conjugation of Stx1 with Alexa Fluor™488 (Molecular Probes, Inc., Eugene, Ore., U.S.A.) was performed according to the manufacturer's protocol. The rat monoclonal antibody (Ab) against Gb3Cer (38.13) was purchased from Beckman/Coulter (Westbrook, Mass., U.S.A.). The mouse monoclonal Ab against Gb3Cer (1A4) was a generous gift of Dr. S. Hakomori of the University of Washington, Seattle, Wash., U.S.A., and Otsuka Assay Laboratories (Kawauchi-cho, Tokushima, Japan). Mouse monoclonal Ab against the Stx1 B-subunit (13C4) was distributed by American Type Culture Collection (ATCC, Rockville, Md., U.S.A.). Secondary Abs, including fluorescein-conjugated Abs and enzyme-conjugated Abs, were purchased from Molecular Probes and Jackson ImmunoResearch Laboratories, Inc. (West Grove, Pa., U.S.A.), respectively. Purified Gb3Cer, globotetraosyl ceramide (Gb4Cer), sodium butyrate, and all other chemical reagents were obtained from Sigma-Aldrich Fine Chemicals (St. Louis, Mo., U.S.A.), unless otherwise indicated.

For cell culture, 2.5–20 mM stocks of Gb4Cer were prepared by dissolving in dimethyl sulfoxide and were added to the culture medium at a 1:1,000 dilution ratio to make the final concentration of 2.5–20 mM. Similarly, 1 M stock of sodium butyrate in phosphate buffered saline (PBS) was added to the culture medium at a 1:1,000 dilution ratio to make the final concentration of 1 mM. For serum starvation, cells were cultured under the condition of 1% FCS for 48 hr prior to the experiments.

Cell viability assay. Vero cells were plated on 96-well plates (Corning, Inc., Corning, N.Y., U.S.A.) at 1×10^4 cells in 100 µl of medium per well to achieve approximately three quarters confluence and they were then allowed to settle by overnight cultivation. After incu-

bation with different concentrations of Stx1 as indicated in each figure for 48 hr, viable cell counts were estimated by a modified methylthiazolyldiphenyl-tetrazolium bromide (MTT) assay as described previously (4), and they were expressed as a percentage of the untreated cell count. Experiments were performed in triplicate, and the means+SD of the values are shown in the figure.

Flow cytometric analysis and detection of apoptosis. For flow cytometry, cell suspensions of Vero cells were produced by treating the cells with trypsin-EDTA and pipetting. Fluorescent immunocytostaining was performed as described previously (2). To detect binding with holotoxin and the B-subunit of Stx1, one million cells in suspension were incubated with 100 ng/ml of Alexa Fluor™488-labeled holotoxin and the B-subunit of Stx1 in 100 µl of medium, respectively, for 30 min at 4 C. After intensive washing with PBS, cells were analyzed by flow cytometry (EPICS-XL, Coulter) as described previously (12, 34). Apoptosis was detected by staining with fluorescein isothiocyanate (FITC)-labeled annexin V for 15 min at room temperature by using an MEBCYTOR®-Apoptosis Kit (Medical & Biological Laboratories Co., Ltd., Nagoya, Aichi, Japan) according to the manufacturer's protocol.

Lipid analysis and TLC-blotting. The lipids were extracted from 1×10^7 of Vero cells with chloroform/methanol (2:1, v/v). The entire lipids were separated on a high performance thin-layer chromatography (TLC) plate (Merck, Darmstadt, Germany) in a chloroform/methanol/0.2% $CaCl_2$ (60:35:8, v/v/v) solvent system and visualized by spraying orcinol/H_2SO_4, as described previously (9). As a control, 1 µg each of the standard lipids of LacCer, Gb3Cer, and Gb4Cer were separated on a TLC plate simultaneously and the position of each lipid was indicated in the figure.

TLC-blotting for the detection of Stx1 binding was performed as described previously (9). Briefly, entire lipids extracted from 1×10^6 of Vero cells were separated on a TLC plate as described above and were transferred to a PVDF membrane, followed by blocking with 5% skimmed milk in PBS. After incubation with Stx1 B-subunit at 100 ng/ml for 30 min at room temperature, the membrane was washed with PBS containing 0.025% Tween 20 (Sigma), incubated with anti-Stx1 B-subunit Ab at 1 µg/ml for 30 min at room temperature, and washed again. After further incubation with peroxidase-conjugated secondary Ab at 1 µg/ml for 30 min at room temperature and the following final washing, the membrane was visualized with enhanced-chemiluminescence (ECL Westernblotting system, Amersham Pharmacia Biotech, U.K. Ltd., Buckinghamshire, U.K.). The results obtained from a 1-min exposure of the ECL-treated membrane to film are presented. TLC-blotting for the detection of Gb3Cer was performed using anti-Gb3Cer Abs in essentially the same manner as described above with an exception of the absence of preincubation with Stx1 B-subunit.

Confocal microscopic analysis of Stx1 incorporated in to the cells. For immunohistochemical detection of incorporated Stx1, 5×10^5 cells in 2 ml of medium were plated on collagen-coated cover slips (Iwaki Glass, Inc., Tokyo) placed in a 35 mm culture dish and grown overnight to achieve approximately a half confluence. At the end of the culture period, Stx1 was bound to the cells by incubation at 100 ng/ml in 1 ml of medium for 30 min at 4 C and then washed intensively with ice-cold PBS to remove the excess toxin. To allow incorporation of the toxin, cells were incubated for 4 hr in a fresh medium with shifts in temperature from 4 C to 37 C. The cover slips were then washed with PBS and fixed with 100% acetone for 15 min at 4 C, followed by incubation with anti-Stx1 Ab 13C4 at 10 µg/ml in 1 ml of medium for 60 min at room temperature and intensive washing with PBS. After incubation with Alexa Fluor™488-conjugated secondary Abs (Molecular Probes) at 10 µg/ml for 30 min and following nuclear counter staining with DAPI (200 ng/ml) for 15 min, the cover slips were washed and mounted on slide glasses using PermaFluor™ Aqueous mounting medium (Thermo Shandon, Pittsburgh, Pa., U.S.A.) and examined by confocal microscope.

For the colocalization analysis of Stx1 with lysosomal marker in R-Vero cells, a 35 mm polylysine-coated glass bottom dish (Matsunami Glass Ind., Ltd., Tokyo) and Alexa Fluor™488-conjugated Stx1 were used and the toxins were incorporated in a similar procedure as described above while the lysosome-selective probe LysoTracker RED DND-99 (final concentration of 50 nM, Molecular Probes) was added to the medium 1 hr after the temperature shift to 37 C. At the end of incubation, dishes were intensively washed with PBS and cells were mounted using aqueous mounting medium and examined by confocal microscope.

Confocal laser scanning was performed using an FV500 confocal laser scanning microscope (Olympus, Tokyo). Simultaneous multi-fluorescence acquisitions were performed using the 351-nm, 488-nm, and 543-nm laser lines to excite DAPI, Alexa Fluor™488, and RED DND-99, respectively, using a water-immersion objective (×40, NA1.7). Fluorescent images were selected using appropriate multi-fluorescence dichroic mirrors and band pass filters using the sequential acquisition mode.

Results

Identification of the Shiga-Toxin 1-Resistant Stock of Vero Cells

Vero cells have been reported to be highly sensitive to Stx cytotoxicity (14), and the Vero cells stored in our laboratory {designated as sensitive (S-) Vero in this paper for convenience} display high sensitivity to Stx1, and their cell viability is markedly reduced in a time and dose-dependent manner after Stx1 treatment. As shown in Fig. 1A, after treatment for 48 hr, 10 pg/ml of Stx1 induced about an 80% reduction in the number of cells as assessed by MTT assay. Previous reports, including our own, have indicated that apoptosis is involved in the process of Stx-mediated cell death (6, 18, 34, 38). As shown in Fig. 1B, flow cytometric analysis revealed that 62.4% of S-Vero cells bound to annexin V after a 48-hr treatment with 10 pg/ml of Stx1, suggesting a significant induction of apoptosis in S-Vero cells.

In the process of comparing the Stx1 sensitivity of different stocks of Vero cells, however, we found that the stock of Vero cells distributed by the Institute for Fermentation {designated resistant (R-) Vero in this paper for convenience} exhibit low sensitivity to Stx1. As shown in Fig. 1A, after treatment for 48 hr, 10 pg/ml of Stx1 induced only about a 20% reduction in the number of cells, as assessed by MTT assay. Even at a higher concentration, 100 pg/ml, approximately 75% of the cells were still viable (Fig. 1A). In parallel, flow cytometric analysis revealed that only 22.9% of the R-Vero cells bound to annexin V after 48-hr treatment with 10 pg/ml of Stx1 (Fig. 1B). The data indicate reduced sensitivity of R-Vero cells to Stx1. We also tested Stx2 cytotoxicity against both S- and R-Vero cells and essentially observed results similar as to those for Stx1 (data not shown).

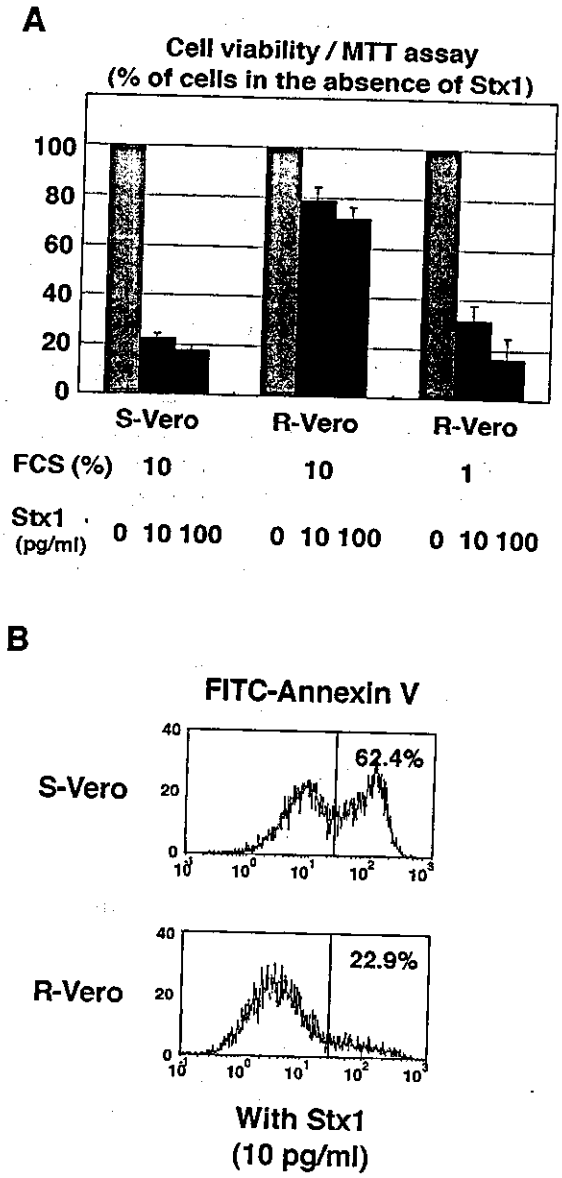

Fig. 1. Susceptibility of different stocks of Vero cells to Shiga toxin 1 (Stx1) cytotoxicity. A: After 48 hr of incubation with different concentrations of Stx1, viable cell counts of sensitive (S-) and resistant (R-) Vero cells were estimated by MTT assay. Two different concentrations of FCS, 10% and 1%, were tested on R-Vero cells as described in "Materials and Methods." B: Vero cells treated in the same manner as in A. After incubation, apoptotic cells were detected by annexin V-binding assay using flow cytometry. The resulting histograms show the percentages of annexin V-bound cells. X-axis, fluorescence intensity; Y-axis, relative cell number.

Distinct Gb3Cer Expression in the Shiga-Toxin 1-Resistant Stock of Vero Cells

Next, we measured the level of expression of Gb3Cer in S- and R-Vero cells by several different methods. When the expression level of Gb3Cer was measured by flow cytometry with anti-Gb3Cer 38.13 mAbs, the S-Vero cells showed a heterogeneous staining pattern, and their fluorescence intensity ranged from very weak to strong (Fig. 2). By contrast, when R-Vero cells were similarly tested, they showed only weak staining with 38.13 mAb (Fig. 2). When we tested another anti-Gb3Cer mAb, 1A4, we observed identical results (Fig. 2). Curiously, however, when binding of FITC-labeled Stx1 was examined by flow cytometry, the results showed significant binding of Stx1 by R-Vero cells (Fig. 2). As shown in Fig. 2, some of the R-Vero cells showed stronger fluorescence intensity after incubation with FITC-Stx1 than the S-Vero cells. We obtained similar results when we tested binding of the FITC-labeled B-subunit of Stx1 (Fig. 2).

The above results may seem to suggest that R-Vero

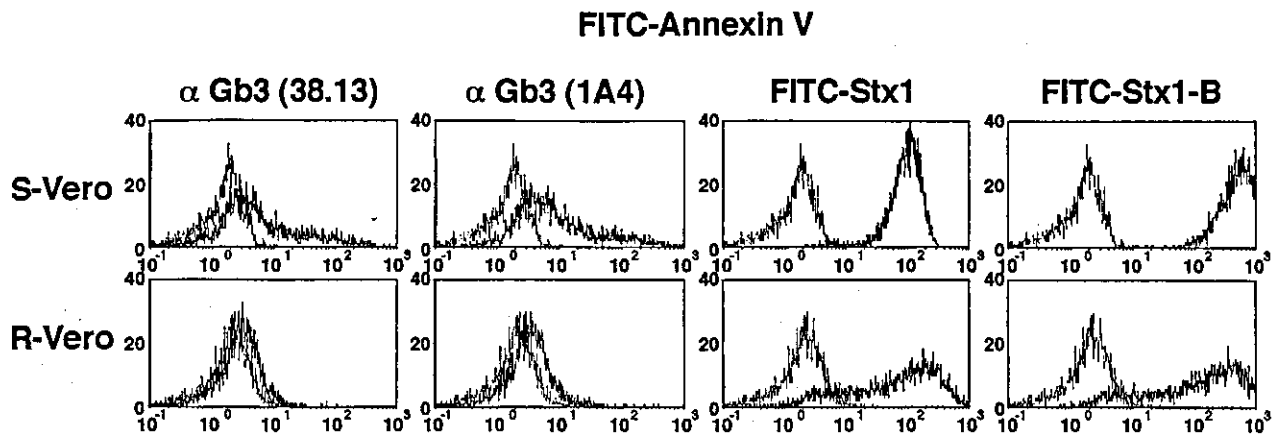

Fig. 2. Expression of globotriaosyl ceramide (Gb3Cer) and cell surface binding of Shiga toxin 1 (Stx1). Cell suspensions obtained from sensitive (S-) (upper panel) and resistant (R-) Vero cells (lower panel) were incubated with FITC-labeled anti-Gb3Cer monoclonal antibodies or Alexa Fluor™488-conjugated holotoxin and the B-subunit of Stx1, and analyzed by flow cytometry. The histogram obtained has been superimposed on that of the negative control. X-axis, fluorescence intensity; Y-axis, relative cell number.

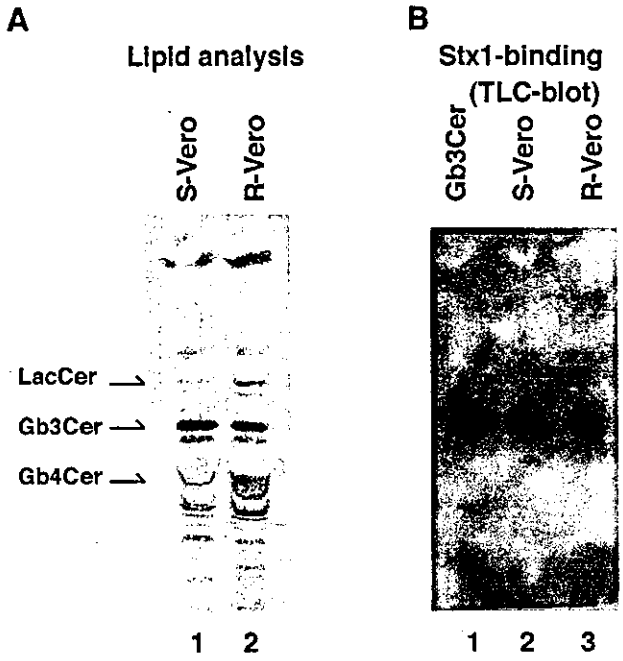

Fig. 3. Lipid analysis of Vero crlls. A: The lipids of sensitive (S-) (left lane) and resistant (R-) Vero cells (right lane) were analyzed as described in "Materials and Methods." B: Binding of Shiga toxin 1 (Stx1) to lipids extracted from S- (mid lane) and R-Vero cells (right lane) was assessed by TLC-blotting. As a control, purified globotriaosyl ceramide was tested at the same time (left lane).

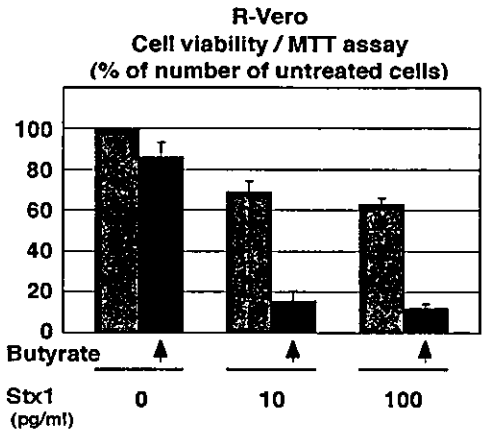

Fig. 4. Effect of sodium butyrate on the Shiga toxin 1 (Stx1) sensitivity of Vero cells. Resistant (R-) Vero cells pre-incubated and not incubated with 1 mM of sodium butyrate for 24 hr were exposed to Stx1for 48 hr. The number of viable cells was determined by MTT assay as in Fig. 1A.

cells express other receptor(s) for Stx1 and may not express Gb3Cer. However, as shown in Fig. 3A, lipid analysis revealed that almost the same amount of Gb3Cer was expressed by the R-Vero cells as by the S-Vero cells. In addition, TLC-blotting analysis revealed that Stx1 only binds Gb3Cer and no other components of the lipids extracted from either R- or S-Vero cells (Fig. 3B). Moreover, both anti-Gb3Cer Abs could recognize Gb3Cer extracted from R-Vero cells similary as that from S-Vero cells in TLC-blotting (data not shown). Therefore, it seems most likely that R-Vero cells express a considerable amount of Gb3Cer on the cell surface, and thus bind with Stx1, but that the anti-Gb3Cer Ab binding site in Gb3Cer is conformationally masked by an unknown modification specifically present in the cell membrane of R-Vero cells. It is noteworthy that the amounts of LacCer and Gb4Cer are higher in R-Vero cells than in S-Vero cells (Fig. 3A).

Effect of Butyrate, Serum Depletion, and Exogenous Gb4Cer on Stx1 Cytotoxicity against Vero Cells

Since treatment with butyrate has been reported to

enhance cell sensitivity to Stx cytotoxicity (31), next, we investigated whether treatment with butyrate affects the cytotoxic effect of Stx1 on R-Vero cells. Interestingly, when 1 mM sodium butyrate was added to the medium 24 hr prior to the challenge of the toxin, the sensitivity of R-Vero cells to Stx1 cytotoxicity significantly increased, and 10 pg/ml of Stx1 induced a more than 90% reduction in the number of cells after 48 hr of incubation, as assessed by MTT assay (Fig. 4A).

We also investigated whether serum depletion affects the cytotoxic effect of Stx1 on R-Vero cells. When R-Vero cells cultured under low serum conditions of 1% FCS for 48 hr were treated with Stx1, Stx1 cytotoxicity was significantly enhanced, and more than a 60% and 80% reduction in the number of cells was observed by MTT assay after 48-hr incubation with 10 and 100 pg/ml Stx1, respectively (Fig. 1A).

In parallel, we measured the Gb3Cer expression level in serum depleted R-Vero cells by flow cytometry and compared it with that in R-Vero cells under regular culture conditions with 10% FCS that was indicated in Fig. 2. However, no significant change was observed in both staining patterns with anti-Gb3Cer Abs and binding of Stx1 (data not shown), suggesting that serum depletion does not affect the expression level of Gb3Cer in R-Vero cells.

Since we observed an increased level of Gb4Cer in R-Vero cells, next, we investigated whether an addition of exogenous Gb4Cer would affect Stx1 cytotoxicity against S-Vero cells. As shown in Fig. 5, when S-Vero cells were incubated with culture medium containing 10 μM of Gb4Cer for 24 hr prior to Stx1 treatment, Stx1 cytotoxicity assessed by annexin V-binding assay was slightly, but clearly, decreased. In an attempt to see the more significant inhibition of Stx1 cytotoxicity mediated by Gb4Cer, we tested different experimental conditions. As shown in Fig. 5B, the inhibitory effect tended to be dependent on the Gb4Cer dose. However, increasing amounts of Gb4Cer did not result in significant enhancement of apoptosis inhibition even if the amount of Stx1 was decreased. The data indicate that the effect of exogenous Gb4Cer on Stx1 cytotoxicity is limited.

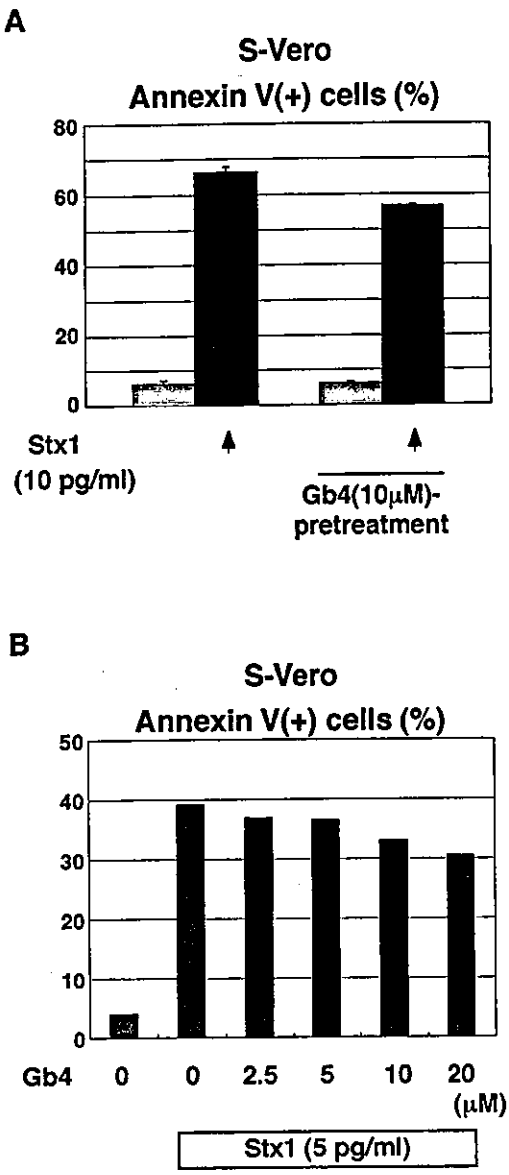

Fig. 5. Effect of endogenous Gb4Cer on the Shiga toxin 1 (Stx1) sensitivity of Vero cells. A: Sensitive (S-) Vero cells pre-incubated and not incubated with 10 μM Gb4Cer for 24 hr were exposed to Stx1 for 48 hr. FITC-annexin V binding was assessed as in Fig. 1B. Experiments were performed in triplicate, and the means+SD of the values are indicated. B: S-Vero cells pre-incubated and not incubated with Gb4Cer at the different concentrations as indicated in the figure for 24 hr were exposed to 5 pg/ml of Stx1 for 48 hr. FITC-annexin V binding was assessed as in A.

Fig. 6. Localization of incorporated Shiga toxin 1 (Stx1) in sensitive (S-) and resistant (R-) Vero cells. A: Stx1 incorporated in S- and R-Vero cells were stained with the combination of anti-Stx1 antibody 13C4 and Alexa Fluor™488-conjugated secondary antibody (green) as described in "Materials and Methods." Nuclei were counterstained with DAPI (blue). Incorporated Stx1 was visualized by confocal microscopy. The peri-nuclear localizations of Stx1 were indicated by arrows. B: Stx1 incorporated in A431 cells was detected as in A. C: The localizations of incorporated Stx1 (green) and a lysosomal marker LysoTracker RED DND-99 (red) in R-Vero cells were simultaneously examined by confocal microscopy as described in "Materials and Methods." In the bottom panel, both images were superimposed with nuclear staining (blue).

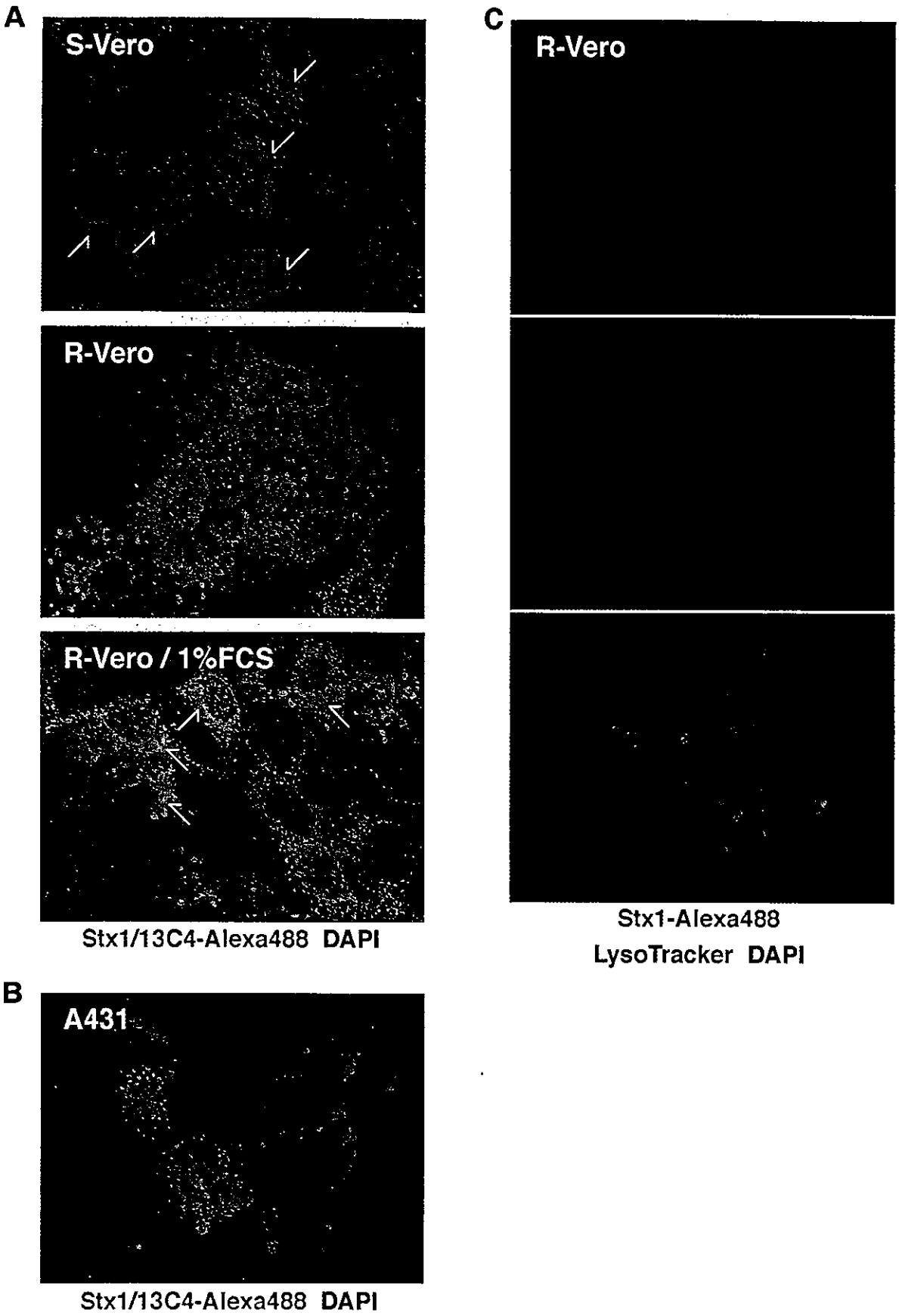
A
S-Vero
R-Vero
R-Vero / 1%FCS
Stx1/13C4-Alexa488 DAPI
B
A431
Stx1/13C4-Alexa488 DAPI
C
R-Vero
Stx1-Alexa488
LysoTracker DAPI

Fig. 6.

Different Intracellular Transport of Stx1 in S- and R-Vero Cells

Stx1 may be able to bind R-Vero cells but not be incorporated by them, with the cells escaping cell death as a result. To test this possibility, we used confocal laser scanning microscopy to determine whether fluorescein-conjugated Stx1 is incorporated by S- and R-Vero cells. As shown in Fig. 6A (upper panel), Stx1 was incorporated into the S-Vero cells and transported to the peri-nuclear area after 4 hr (pointed by arrows). Interestingly, Stx1 was also incorporated significantly by the R-Vero cells, but the localization of the toxin was different from its localization in S-Vero cells. As shown in Fig. 6A (mid panel), the Stx1 incorporated into the R-Vero cells exhibited a granular pattern within the cytoplasm. We also examined the effect of serum depletion on the intracellular transport of Stx1 in R-Vero cells. As shown in Fig. 6A (lower panel), when Stx1 was incorporated in R-Vero cells precultured under the condition of 1% FCS for 48 hr, an increase in the number of the cells in which Stx1 localized in peri-nuclear area was observed (pointed by arrows). The date suggests that the serum depletion affects the intracellular transport of Stx1 in R-Vero cells.

As we mentioned above, the existence of an alternate route of toxin transport to the lysosomes for degradation in some cells, such as A431 cells, has been reported (32). As shown in Fig. 6B, when we examined the localization of Stx1 in A431 cells, the incorporated toxin exhibited a granular pattern within the cytoplasm similar to that in R-Vero cells. Therefore, we examined whether incorporated Stx1 in R-Vero cells colocalize with the lysosomal marker. When the intracellular localization of Alexa Fluor™488-conjugated Stx1 and the lysosome-selective probe LysoTracker RED DND-99 in R-Vero cells were simultaneously examined, the colocalization of these molecules was observed (Fig. 6C). The data suggest that a large propotion of the Stx1 incorporated in R-Vero cells is transported to lysosomes under the regular culture condition with 10% FCS.

Discussion

In this study, we demonstrated the existence of an Stx1-resistant stock of Vero cells. Although Stx1-resistant cell clones of Vero cells have been reported by other groups, the mechanism of the Stx1 resistance in our R-Vero cells and others seems to be different. For example, Kongmuang et al. reported Stx-resistant Vero cells that were isolated by treating the cells with nitrosoguanidine and had lost their toxin-binding capacity as assessed by immunofluorescent analysis (13). Pudymaitis et al. reported a Stx-resistant Vero cell clone that was isolated by its ability to grow in the presence of Stx2 at a concentration of approximately 7 ng/ml and was found to be deficient in Gb3Cer (28). Therefore, the main mechanism of the Stx resistance in the previous examples of Stx-resistant Vero cell clones was a lack of toxin-binding capacity, whereas as shown in this report, our Stx1-resistant Vero cells express an amount of Gb3Cer comparable to that of Stx1-sensitive Vero cells and possess considerable toxin-binding capacity. Indeed, we confirmed significant toxin incorporation into the R-Vero cells by confocal microscopic study (Fig. 6).

Interestingly, Sandvig et al. demonstrated another mechanism of Stx resistance (31). They reported that cell line A431 derived from epidermoid carcinoma, which expresses Gb3Cer and has toxin-binding capacity, is completely resistant to Stx. However, A431 cells acquire Stx sensitivity when cultured in the presence of butyrate, and the mechanism of their distinct sensitivity to Stx cytotoxicity is explained by an alteration in the transport route of Stx after receptor-mediated endocytosis. It has been well documented that retrograde transport of Stx into cytoplasm, where Stx cleaves RNA, is required for expression of cytotoxicity by Stx (17, 31). Under regular culture conditions, most of the toxins in A431 cells resistant to Stx are transported to the lysosomes and degraded, thereby destroying its cytotoxicity. In butyrate-treated A431 cells, however, internalized toxins are routed to the cytoplasm through the Golgi network and endoplasmic reticulum, and thus they exhibited significant sensitivity to Stx cytotoxicity (31). Although further investigations are needed, the mechanism of the Stx1 resistance that we observed in R-Vero cells may be the same as in A431 cells. Our finding of different localizations of the Stx1 incorporated into R- and S-Vero cells, of Stx1 colocalization with the lysosomal marker in R-Vero cells, and of butyrate-mediated sensitization of R-Vero cells to Stx1 should support this notion.

It is noteworthy that Stx1 bound to the Gb3Cer expressed on the cell surface of the R-Vero cells, whereas anti-Gb3Cer monoclonal Ab showed less ability to bind to Gb3Cer. Previously, Lingwood and co-worker demonstrated that the fatty acid composition of Gb3Cer influences its ability to bind to ligands. For example, Gb3Cer containing fatty acid species shorter than C14 were found to be ineffective as receptors for Stx in a phosphoplipid matrix, whereas when fatty acids longer than C20 were used, the species were effectively recognized by Stx but were no longer substrates for galactose oxidase (26), indicating that different epitopes required by these two different ligands (Stx and galactose oxidase) are differentially expressed on different Gb3Cer fatty acid homologues (1, 41). Considering their reports,

it seems to be a plausible explanation that the difference in fatty acid composition of Gb3Cer between R- and S-Vero cells may exist and affect the recognition of Gb3Cer by anti-Gb3Cer monoclonal Abs, but not by Stx1. However, they also reported that the fatty-acid length influences the mobility of Gb3Cer in TLC (11). Since no significant difference was observed in the mobility between Gb3Cer of R-Vero and that of S-Vero in our TLC result (Fig. 3), fatty-acid lengths of both Gb3Cer are not significantly different. Therefore, the failure of the recognition of Gb3Cer expressed on R-Vero cells by the anti-Gb3Cer monoclonal Abs may not be explained by the difference in fatty acid composition. In addition, we also observed that anti-Gb3Cer antibodies could recognize Gb3Cer of R-Vero similar to that of S-Vero cells in the TLC-blot (data not shown). Although the precise reason is unknown, Gb3Cer expressed R-Vero cells are not compositionally different from that of S-Vero cells, but presented differently on the cell surface and the anti-Gb3Cer Ab binding site in Gb3Cer is conformationally masked by an unknown modification specifically present in the cell membrane of R-Vero cells.

We also observed a difference in lipid composition between R- and S-Vero cells. The amounts of both LacCer and Gb4Cer were higher in R-Vero cells than in S-Vero cells, but the amount of Gb3Cer was unchanged (Fig. 3A). Furthermore, as we showed in this study, addition of exogenous Gb4Cer reduced the Stx1 sensitivity of S-Vero cells. It was reported that purified gangliosides exogenously added to the culture medium bind and are stably incorporated in cultured cells (25). In addition, the incorporated exogenous gangliosides are thought to function as components of cell membranes (16, 27). The evidence should support the notion that preincubation of cells with exogenous glycosphingolipids is a reasonable approach to enrich cellular glycosphingolipids. Therefore, the inhibitory effect of exogenous Gb4Cer on Stx1-induced apoptosis in S-Vero cells may be a consequence of the enrichment of Gb4Cer in the cell membrane and suggest a correlation between lipid composition and Stx1 susceptibility. Although the details are unknown, the differences in lipid composition of the cell membrane may affect Gb3Cer recognition by ligands and the sorting route of incorporated Stx1. Since we also found that serum starvation increases the susceptibility of cells to Stx1 cytotoxicity, the serum concentration of the culture medium may affect the lipid composition of the cell membrane.

In conclusion, we have reported a stock of Vero cells that has the capacity to bind Stx1 but are significantly resistant to Stx1 cytotoxicity. Additional fundamental studies are clearly necessary, but clarification of the acquisition mechanism of resistance to Stx1 cytotoxicity by these cells should allow a better understanding of the molecular basis of Stx1-mediated cell damage and open the way to improved therapeutic approaches to diseases caused by Stx1.

We thank M. Sone and S. Yamauchi for their excellent secretarial work. We thank Dr. S. Hakomori and Otsuka Assay Laboratories for donating CD77 monoclonal Ab 1A4.

This work was supported in part by Health and Labour Sciences Research Grants from the Ministry of Health, Labour and Welfare of Japan and MEXT. KAKENHI 15019129, JSPS. KAKENHI 15390133 and 15590361. This work was also supported by a grant from the Japan Health Sciences Foundation for Research on Health Sciences Focusing on Drug Innovation. Additional support was provided by a grant from Sankyo Foundation of Life Science.

References

1) DeGrandis, S., Law, H., Brunton, J., Gyles, C., and Lingwood, C.A. 1989. Globotetraosylceramide is recognized by the pig edema disease toxin. J. Biol. Chem. **264**: 12520–12525.
2) Fujimoto, J., Ishimoto, K., Kiyokawa, N., Tanaka, S., Ishii, E., and Hata, J. 1988. Immunocytological and immunochemical analysis on the common acute lymphoblastic leukemia antigen (CALLA) : evidence that CALLA on ALL cells and granulocytes are structurally related. Hybridoma **7**: 227–236.
3) Garred, O., Dubinina, E., Holm, P.K., Olsnes, S., van Deurs, B., Kozlov, J.V., and Sandvig, K. 1995. Role of processing and intracellular transport for optimal toxicity of Shiga toxin and toxin mutants. Exp. Cell Res. **218**: 39–49.
4) Hansen, M.B., Nielsen, S.E., and Berg, K. 1989. Re-examination and further development of a precise and rapid dye method for measuring cell growth/cell kill. J. Immunol. Methods **119**: 203–210.
5) Hughes, A.K., Stricklett, P.K., and Kohan, D.E. 1998. Cytotoxic effect of Shiga toxin-1 on human proximal tubule cells. Kidney Int. **54**: 426–437.
6) Inward, C.D., Williams, J., Chant, I., Crocker, J., Milford, D.V., Rose, P.E., and Taylor, C.M. 1995. Verocytotoxin-1 induces apoptosis in vero cells. J. Infect. **30**: 213–218.
7) Kaplan, B.S., Cleary, T.G., and Obrig, T.G. 1990. Recent advances in understanding the pathogenesis of the hemolytic uremic syndromes. Pediatr. Nephrol. **4**: 276–283.
8) Karpman, D., Hakansson, A., Perez, M.T., Isaksson, C., Carlemalm, E., Caprioli, A., and Svanborg, C. 1998. Apoptosis of renal cortical cells in the hemolytic-uremic syndrome: *in vivo* and *in vitro* studies. Infect. Immun. **66**: 636–644.
9) Katagiri, U.Y., Mori, T., Nakajima, H., Katagiri, C., Taguchi, T., Takeda, T., Kiyokawa, N., and Fujimoto, J. 1999. Activation of Src family kinase Yes induced by Shiga toxin binding to globotriaosyl ceramide (Gb3/CD77) in low density, detergent-insoluble microdomains. J. Biol. Chem. **274**: 35278–35282.

10) Kaye, S.A., Louise, C.B., Boyd, B., Lingwood, C.A., and Obrig, T.G. 1993. Shiga toxin-associated hemolytic uremic syndrome: interleukin-1β enhancement of Shiga toxin cytotoxicity toward human vascular endothelial cells *in vitro*. Infect. Immun. **61**: 3886–3891.
11) Kiarash, A., Boyd, B., and Lingwood, C.A. 1994. Glycosphingolipid receptor function is modified by fatty acid content. Verotoxin 1 and verotoxin 2c preferentially recognize different globotriaosyl ceramide fatty acid homologues. J. Biol. Chem. **269**: 11138–11146.
12) Kiyokawa, N., Taguchi, T., Mori, T., Uchida, H., Sato, N., Takeda, T., and Fujimoto, J. 1998. Induction of apoptosis in normal human renal tubular epithelial cells by *Escherichia coli* Shiga toxins 1 and 2. J. Infect. Dis. **178**: 178–184.
13) Kongmuang, U., Honda, T., and Miwatani, T. 1988. Isolation of Shiga toxin-resistant Vero cells and their use for easy identification of the toxin. Infect. Immun. **56**: 2491–2494.
14) Konowalchuk, J., Speirs, J.I., and Stavric, S. 1977. Vero response to a cytotoxin of *Escherichia coli*. Infect. Immun. **18**: 775–779.
15) Kozlov, Y.V., Kabishev, A.A., Lukyanov, E.V., and Bayev, A.A. 1988. The primary structure of the operons coding for *Shigella dysenteriae* toxin and temperature phage H30 shiga-like toxin. Gene **67**: 213–221.
16) Li, R., Manela, J., Kong, Y., and Ladisch, S. 2000. Cellular gangliosides promote growth factor-induced proliferation of fibroblasts. J. Biol. Chem. **275**: 34213–34223.
17) Lingwood, C.A. 1996. Role of verotoxin receptors in pathogenesis. Trends Microbiol. **4**: 147–153.
18) Mangeney, M., Lingwood, C.A., Taga, S., Caillou, B., Tursz, T., and Wiels, J. 1993. Apoptosis induced in Burkitt's lymphoma cells via Gb3/CD77, a glycolipid antigen. Cancer Res. **53**: 5314–5319.
19) Melton-Celsa, A.R., and O'Brien, A.D. 1998. *Escherichia coli* O157:H7 and other Shiga toxin-producing *E. coli* strains, p. 121–128. *In* Kaper, J.B., and O'Brien, A.D. (eds), Structure, biology, and relative toxicity of Shiga toxin family members for cells and animals, ASM Press, Washington, D.C.
20) Mizuguchi, M., Tanaka, S., Fujii, I., Tanizawa, H., Suzuki, Y., Igarashi, T., Yamanaka, T., Takeda, T., and Miwa, M. 1996. Neuronal and vascular pathology produced by verocytotoxin 2 in the rabbit central nervous system. Acta Neuropathol. (Berl.) **91**: 254–262.
21) Nakajima, H., Katagiri, Y.U., Kiyokawa, N., Taguchi, T., Suzuki, T., Sekino, T., Mimori, K., Saito, M., Nakao, H., Takeda, T., and Fujimoto, J. 2001. Single-step method for purification of Shiga toxin-1 B subunit using receptor-mediated affinity chromatography by globotriaosylceramide-conjugated octyl sepharose CL-4B. Protein Expr. Purif. **22**: 267–275.
22) Noda, M., Yutsudo, T., Nakabayashi, N., Hirayama, T., and Takeda, Y. 1987. Purification and some properties of Shiga-like toxin from *Escherichia coli* O157: H7 that is immunologically identical to Shiga toxin. Microb. Pathog. **2**: 339–349.
23) Obrig, T.G., Del-Vecchio, P.J., Brown, J.E., Moran, T.P., Rowland, B.M., Judge, T.K., and Rothman, S.W. 1988. Direct cytotoxic action of Shiga toxin on human vascular endothelial cells. Infect. Immun. **56**: 2373–2378.
24) Ohmi, K., Kiyokawa, N., Takeda, T., and Fujimoto, J. 1998. Human microvascular endothelial cells are strongly sensitive to Shiga toxins. Biochem. Biophys. Res. Commun. **251**: 137–141.
25) Olshefski, R., and Ladisch, S. 1996. Intercellular transfer of shed tumor cell gangliosides. FEBS Lett. **386**: 11–14.
26) Pellizzari, A., Pang, H., and Lingwood, C.A. 1992. Binding of verocytotoxin 1 to its receptor is influenced by differences in receptor fatty acid content. Biochemistry **31**: 1363–1370.
27) Prinetti, A., Iwabuchi, K., and Hakomori, S. 1999. Glycosphingolipid-enriched signaling domain in mouse neuroblastoma Neuro2a cells. Mechanism of ganglioside-dependent neuritogenesis. J. Biol. Chem. **274**: 20916–20924.
28) Pudymaitis, A., Armstrong, G., and Lingwood, C.A. 1991. Verotoxin-resistant cell clones are deficient in the glycolipid globotriosylceramide: differential basis of phenotype. Arch. Biochem. Biophys. **286**: 448–452.
29) Richardson, S.E., Karmali, M.A., Becker, L.E., and Smith, C.R. 1988. The histopathology of the hemolytic uremic syndrome associated with verocytotoxin-producing *Escherichia coli* infections. Hum. Pathol. **19**: 1102–1108.
30) Richardson, S.E., Rotman, T.A., Jay, V., Smith, C.R., Becker, L.E., Petric, M., Olivier, N.F., and Karmali, M.A. 1992. Experimental verocytotoxemia in rabbits. Infect. Immun. **60**: 4154–4167.
31) Sandvig, K., Garred, O., Prydz, K., Kozlov, J.V., Hansen, S.H., and van Deurs, B. 1992. Retrograde transport of endocytosed Shiga toxin to the endoplasmic reticulum. Nature **358**: 510–512.
32) Sandvig, K., and van Deurs, B. 1996. Endocytosis, intracellular transport, and cytotoxic action of Shiga toxin and ricin. Physiol. Rev. **76**: 949–966.
33) Simon, M., Cleary, T.G., Hernandez, J.D., and Abboud, H.E. 1998. Shiga toxin 1 elicits diverse biologic responses in mesangial cells. Kidney Int. **54**: 1117–1127.
34) Taguchi, T., Uchida, H., Kiyokawa, N., Mori, T., Sato, N., Horie, H., Takeda, T., and Fujimoto, J. 1998. Verotoxins induce apoptosis in human renal tubular epithelium derived cells. Kidney Int. **53**: 1681–1688.
35) Takeda, T., Dohi, S., Igarashi, T., Yamanaka, T., Yoshiya, K., and Kobayashi, N. 1993. Impairment by verotoxin of tubular function contributes to the renal damage seen in haemolytic uraemic syndrome. J. Infect. **27**: 339–341.
36) Tesh, V.L., Samuel, J.E., Perera, L.P., Sharefkin, J.B., and O'Brien, A.D. 1991. Evaluation of the role of Shiga and Shiga-like toxins in mediating direct damage to human vascular endothelial cells. J. Infect. Dis. **164**: 344–352.
37) Tesh, V.L., Ramegowda, B., and Samuel, J.E. 1994. Purified Shiga-like toxins induce expression of proinflammatory cytokines from murine peritoneal macrophages. Infect. Immun. **62**: 5085–5094.
38) Uchida, H., Kiyokawa, N., Taguchi, T., Horie, H., Fujimoto, J., and Takeda, T. 1999. Shiga toxins induce apoptosis in pulmonary epithelium derived cells. J. Infect. Dis. **180**: 1902–1911.
39) van Setten, P.A., Monnens, L.A., Verstraten, R.G., van den Heuvel, L.P., and van Hinsbergh, V.W. 1996. Effects of verocytotoxin-1 on nonadherent human monocytes: binding

characteristics, protein synthesis, and induction of cytokine release. Blood **88**: 174–183.

40) van Setten, P.A., van Hinsbergh, V.W., Van den Heuvel, L.P., van der Velden, T.J., van de Kar, N.C., Krebbers, R.J., Karmali, M.A., and Monnens, L.A. 1997. Verocytotoxin inhibits mitogenesis and protein synthesis in purified human glomerular mesangial cells without affecting cell viability: evidence for two distinct mechanisms. J. Am. Soc. Nephrol. **8**: 1877–1888.

41) Yiu, S.C., and Lingwood, C.A. 1992. Polyisobutylmethacrylate modifies glycolipid binding specificity of verotoxin 1 in thin-layer chromatogram overlay procedures. Anal. Biochem. **202**: 188–192.